NeuroImage 246 (2022) 118763

Contents lists available at ScienceDirect

NeuroImage

journal homepage: www.elsevier.com/locate/neuroimage

Stationary EEG pattern relates to large-scale resting state networks – An EEG-fMRI study connecting brain networks across time-scales

J. Daniel Arzate-Mena[a], Eugenio Abela[c], Paola V. Olguín-Rodríguez[j], Wady Ríos-Herrera[i,f], Sarael Alcauter[h], Kaspar Schindler[d], Roland Wiest[e], Markus F. Müller[b,f,g,1], Christian Rummel[e,1,*]

[a] Instituto de Investigación en Ciencias Básicas y Aplicadas, Universidad Autónoma del Estado de Morelos,Cuernavaca Morelos, Mexico
[b] Centro de Investigación en Ciencias, Universidad Autónoma del Estado de Morelos (UAEM), Cuernavaca, Morelos, Mexico
[c] Center for Neuropsychiatrics, Psychiatric Services Aargau AG, Windisch, Switzerland
[d] Department of Neurology, Inselspital, Bern University Hospital, University of Bern, Bern, Switzerland
[e] Support Center for Advanced Neuroimaging, University Institute for Diagnostic and Interventional Neuroradiology, Inselspital, Bern University Hospital, University of Bern, Bern, Switzerland
[f] Centro de Ciencias de la Complejidad (C3), Universisdad Nacional Autónoma de México, Mexico City 04510, Mexico
[g] Centro Internacional de Ciencias A. C., Cuernavaca, México
[h] Instituto de Neurobiología, Universidad Nacional Autónoma de México, Querétaro, México
[i] Facultad de Psicología Universidad Nacional Autónoma de México, Mexico City, Mexico
[j] Instituto de Neurociencias, Universidad de Guadalajara, Guadalajara, Mexico

ARTICLE INFO

Keywords:
Functional magnetic resonance imaging
Electroencephalogram
Independent component analysis
Default mode network
Executive control network
Salience network
Complexity and criticality

ABSTRACT

Relating brain dynamics acting on time scales that differ by at least an order of magnitude is a fundamental issue in brain research. The same is true for the observation of stable dynamical structures in otherwise highly non-stationary signals. The present study addresses both problems by the analysis of simultaneous resting state EEG-fMRI recordings of 53 patients with epilepsy. Confirming previous findings, we observe a generic and temporally stable average correlation pattern in EEG recordings. We design a predictor for the General Linear Model describing fluctuations around the stationary EEG correlation pattern and detect resting state networks in fMRI data. The acquired statistical maps are contrasted to several surrogate tests and compared with maps derived by spatial Independent Component Analysis of the fMRI data. By means of the proposed EEG-predictor we observe core nodes of known fMRI resting state networks with high specificity in the default mode, the executive control and the salience network. Our results suggest that both, the stationary EEG pattern as well as resting state fMRI networks are different expressions of the same brain activity. This activity is interpreted as the dynamics on (or close to) a stable attractor in phase space that is necessary to maintain the brain in an efficient operational mode. We discuss that this interpretation is congruent with the theoretical framework of complex systems as well as with the brain's energy balance.

1. Introduction

The human brain is one of the most complex systems we know. It consists of about 10^{11} elementary building blocks - the neurons, each of them connected with 10^3 to 10^4 others, which constitutes an enormously large network. The total length of the connections (the sum of all axon and dendrite lengths) is about 10 million kilometers (Schelter et al., 2008), which suffices to wrap more than 200 times around the equator. Notwithstanding, it is an extremely sparse network, considering that less than the 10millionth part of all possible connections are actually realized. In order to ensure an efficient information transfer between different (probably distant) brain regions, a special *network topology* is required (Bassett and Bullmore, 2006; Bullmore and Sporns, 2009; Eguiluz et al., 2005; Sporns et al., 2000). This is realized via a hierarchical arrangement of feedback loops, beginning from the microscopic level of modules consisting of a few neurons to the macroscopic scales like the Thalamo-Cortical system, with non-linear interactions within and between the hierarchical levels (Buzsaki, 2006).

The complexity of the neural network is also reflected in its *dynamical* features, like the existence of scaling laws (Eguiluz et al., 2005; Fraiman et al., 2009) and in particular its highly non-stationary nature (Andrzejak et al., 2012). Ever changing internal conditions as well as continuously alternating external stimuli in addition to dynamical noise components provoke unceasing transitions between qualitatively different spatial synchronization patterns of neural populations.

* Corresponding author.
E-mail address: crummel@web.de (C. Rummel).
[1] MFM and CR share senior authorship.

https://doi.org/10.1016/j.neuroimage.2021.118763.
Received 20 March 2021; Received in revised form 17 November 2021; Accepted 24 November 2021
Available online 1 December 2021.

All above mentioned properties are typical for many complex adaptive systems, and, counter intuitively, they are capable to generate characteristic structures that are surprisingly stable in time (Hastings, 1984; Münnix et al., 2012; Schneider and Somers, 2006; Wollin and Perry, 2004). These structures may act as a kind of dynamical scaffold around which a system evolves.

Evidently, such a dynamical backbone within otherwise highly non-stationary signals is of major importance for the understanding of the corresponding system. Studying its properties may reveal fundamental principles of its complex dynamics, similar to the attractor topology of dynamical systems in phase space. Apparently, also the brain encounters preferential dynamical states, whose underlying network seems to operate close to a critical point (Beggs and Timme, 2012; Chialvo, 2010; Fraiman et al., 2009; Linkenkaer-Hansen et al., 2001; Tagliazucchi et al., 2012).

Functional magnetic resonance imaging (fMRI) has revealed stable interaction patterns in the resting brain, the so called resting state networks (RSN) (Buckner et al., 2013; Damoiseaux et al., 2006; Seitzman et al., 2019; Van Den Heuvel and Pol, 2010; Zang et al., 2012) like the Default Mode Network (DMN) (Raichle et al., 2001), the Salience Network (SN) (Menon and Uddin, 2010), the Sensory-Motor Network (SMN) (Biswal et al., 1995) or the Executive Control Network (ECN) (Seeley et al., 2007) to mention some of the most prominent ones. The study of these dynamical networks opened new avenues of brain research, illuminating fundamental aspects of the basal brain dynamics.

A potential problem of fMRI measurements is the slow hemodynamic response that only allows indirect assessment of neuronal processes on long time scales, i.e. on the order of several seconds (Cordes et al., 2000). However, most of the brain activity occurs on time scales that are orders of magnitude faster, i.e. occur within fractions of a second. These processes are much better captured by electroencephalographic recordings (EEG), which may register the electrical brain activity up to the kilohertz range. Thereby not only much faster spectral components, which are responsible for a plenitude of interesting processes can be investigated, like for instance higher cognitive functions (Başar et al., 1999; Bressler and Tognoli, 2006; Kaiser and Lutzenberger, 2005). Unfortunately, also the non-stationarity of the signals is notably increased.

Still, in Corsi-Cabrera et al. (2007, 1997) pronounced and temporally stable cross-correlations were detected in EEG of healthy women during rest. In repeated measurements over weeks or even months the authors reported high within-subject reliability. Furthermore, the results were homogeneous across each subject group. Also, in Kramer et al. (2011) stable templates have been found in intra-cranial EEG of epilepsy patients employing graph theoretical measures.

Further, the authors of He et al. (2008) reported a stable correlation pattern during wakefulness, slow wave, and rapid eye movement sleep as assessed by electrocorticograms of five epilepsy patients. It turned out that the slow cortical potentials demonstrate a correlation structure similar to the spontaneous fluctuations of blood oxygen-level dependent (BOLD) signals. This is an important observation because it provides a direct link between the electrical brain activity and changes of the blood oxygen levels.

In Müller et al. (2014) focal onset seizures were studied using scalp EEG, concentrating on the peri-ictal transition, i.e. epochs before, during and after seizure occurrence. In contrast to the expectation, the authors found a pronounced non-zero average correlation pattern during the pre-ictal, ictal and the post-ictal periods, which in addition turned out highly similar for the three conditions, in spite of the crucial dynamical changes during the peri-ictal transition. Furthermore, the observed pattern was generic in the sense that also across different subjects a high similarity of the average correlation pattern was observed.

Finally, in Olguín-Rodríguez et al. (2018) scalp EEGs, recorded under quite different conditions like, whole night sleep of healthy subjects, open and closed eyes of healthy young and elderly adults as well as focal onset seizures of epilepsy patients have been considered. Analysis led to the conclusion that (i) the average cross-correlation matrices estimated separately for different physiological (as well as pathological) states are extremely similar, and (ii) this pattern is generic in the sense that it is (almost) subject independent. Taking the evidence in these contributions together, averaging over EEG epochs belonging to different physiological states (like e.g. different sleep stages) is justified. In the following, we denote the resulting average cross-correlation matrix as "Stable Correlation Pattern" (SCP).

In sum, in slow hemodynamic processes as assessed by fMRI as well as in fast electrical brain activity measured by EEG surprisingly stable, generic interrelation patterns have been found. According to these observations, the RSN and the SCP appear to constitute a dynamical backbone, that coordinates the brain activity to respond appropriately to ever changing conditions.

We hypothesize that if the variations of the SCP and BOLD fluctuations in resting state fMRI are different manifestations of the same phenomenon, simultaneous EEG-fMRI measurements (Gotman et al., 2006; van Graan et al., 2015; Nunez and Silberstein, 2000; Ritter and Villringer, 2006; Wiest et al., 2015) should be an appropriate tool to investigate their mutual relationships using the General Linear Model (GLM).

In many applications fluctuations in EEG-power have been used in order to relate fast electrical brain activity with the notably slower BOLD signals (Britz et al., 2010; Goldman et al., 2002; Horovitz et al., 2008; Jann et al., 2010; Laufs et al., 2003; Neuner et al., 2014; Portnova et al., 2018; Prestel et al., 2018; Rajkumar et al., 2018; Samogin et al., 2019), sometimes using frequency components up to 50 Hz (Mantini et al., 2007). However, it was shown that slow modulations of respiration and heart rate below 0.1 Hz may strongly influence the results (Chen et al., 2020; Yuan et al., 2013), certainly an undesired effect.

In contrast, in the present study we investigate the response of BOLD-fMRI to a functional network predictor calculated from bivariate interrelations *between* EEG signals measured at different electrodes and thus representing a functional network. Note that this is conceptually different to e.g. using fluctuations in topographic maps of spectral EEG power (Labounek et al., 2019) or the power fluctuations originated by the so called microstates (Britz et al., 2010; Michel and Koenig, 2018; Rajkumar et al., 2018), which as a univariate quantity calculated for each electrode separately does not reflect signal interrelations without further assumptions. We hypothesize that the intrinsic fluctuations around the SCP in EEG predict activation maps similar to known RSNs of BOLD-fMRI.

2. Materials and methods

2.1. Subjects

Since the SCP has previously been identified as a rather generic pattern with topology insensitive to pathologies (Müller et al., 2014; Olguín-Rodríguez et al., 2018), 53 patients with epilepsy were included in our study, see Tab. S1 of the Supplementary Materials for details. The inclusion criteria were the presence of epileptiform EEG activity, visible on scalp EEG recordings, and referral for simultaneous EEG-fMRI at the University Hospital Bern, Switzerland (Inselspital). Thirty-one patients were female. The mean age ± SD of the group was 36.2 ± 13.4 years and their age ranged from 15 to 68 years. The epilepsy syndromes were clinically evaluated by the referring physicians and included: ideopathic generalized epilepsy (IGE, 13 patients), mesial temporal lobe epilepsy (MTLE, 13 patients), lateral temporal lobe epilepsy (LTLE, 12 patients), frontal lobe epilepsy (FLE, 9 patients), parietal lobe epilepsy (PLE, 3 patients). One patient was diagnosed with West syndrome and one with juvenile myoclonic epilepsy (JME), while another patient had not yet received a diagnosis.

This study was approved by the Ethics Committee of the Canton of Bern (approval no. 2017-00697) and all patients signed informed consent. All clinical decisions were made prior and independent from this retrospective data evaluation.

2.1.1. Paradigm

All EEG and EEG-fMRI measurements were performed at resting state with eyes closed. During the recordings outside the scanner, patients were intermittently asked to open their eyes for 20 s to facilitate the identification of the effect of eye movements.

2.2. MRI

2.2.1. Setup and data acquisition

A Siemens Magnetom Trio TIM MR Scanner (Erlangen, Germany) with magnetic field strength 3 Tesla was used for MRI data acquisition with a 32-channel head coil. Image acquisition was performed in supine position and head motion was minimized by fitting foam pads between head and coil. Scanner noise was reduced by using ear plugs.

All subjects underwent T2*-weighted functional imaging while simultaneously recording EEG (see Section 2.3.1). BOLD data were registered with a standard echo planar imaging (EPI) sequence with the following MR parameters: repetition time (TR) 1980 ms; echo time (TE) 30 ms; flip angle 90°; inversion time (TI) 910 ms; voxel size 3.0 mm × 3.0 mm × 4.0 mm; field of view (FOV) 192 mm (matrix size 64 × 64); slice thickness 4 mm. A total of $N_{vol} = 460$ functional volumes were recorded for each patient (total recording time 15 min 11 s). To avoid contamination of the EEG recordings, the helium pump of the MR scanner was temporarily switched off during this time.

For anatomical co-registration three-dimensional T1-weighted images were obtained in sagittal direction using either the Modified Driven Equilibrium Fourier Transformation (MDEFT Deichmann et al., 2004) sequence or Magnetization Prepared Rapid Acquisition Gradient Echo (MP-RAGE Held et al., 1995). In both cases the voxel size was 1.0 mm × 1.0 mm × 1.0 mm.

2.2.2. MRI preprocessing

Processing of the MRI data was carried out using FSL (FMRIB's Software Library, www.fmrib.ox.ac.uk/fsl), provided by the Functional MRI of the Brain (FMRIB) Analysis Group at University of Oxford, UK. FMRI was analyzed with FEAT (FMRI Expert Analysis Tool), version 6.00. The boundary-based registration (BBR) algorithm (Greve and Fischl, 2009) was used to register the functional data to the high resolution structural image. We applied FLIRT (Jenkinson et al., 2002; Jenkinson and Smith, 2001) and FNIRT (Andersson et al., 2007a; 2007b) to register the high resolution structural MRI to standard space templates for group analyses. Motion correction was accomplished by MCFLIRT (Jenkinson et al., 2002), the slice-timing correction was performed by Fourier-space time-series phase-shifting, non-brain removal was carried out by means of the brain extraction tool (BET) (Smith, 2002), spatial smoothing was accomplished using a Gaussian kernel with full width at half maximum (FWHM) of 6 mm. The data was temporally high-pass filtered with a Gaussian-weighted least-squares straight line fitting with time constant $\sigma = 55.5$ s.

2.3. EEG

2.3.1. Set up and recording

The EEG of all patients was first recorded outside the scanner (duration 10 min) and then inside with simultaneous acquisition of BOLD-fMRI (duration 15 min 11 s). Two MR compatible EEG systems were used. Both amplifiers were battery-powered and connected through optical wires to the data acquisition PC so that the patients' security was guaranteed (Lemieux et al., 1997). The EEG caps of both acquisition systems contained the electrodes of the international 10-10 system as a subset.

A BrainAmp amplifier (Brain Products, Gilching, Germany) was used in 44 patients (patient group A) with an EasyCap and 92 EEG electrodes. In addition, two electrodes were placed under the left and right clavicles to record the electrocardiogram (ECG) and two electrodes were placed below the eyes to record the electrooculogram (EOG). The electrode impedances were kept below 20 kΩ and the electrode at position F_z was used as recording reference. The signals were amplified, band-pass filtered between 0.1 and 250 Hz and digitally stored for offline analysis. Sampling rate was 5 kHz.

In the nine patients of group B a GES 400 MR amplifier (Electrical Geodesics Inc., EGI, Eugene, OR, USA) was used with a 256-channel HydroCel Geodesic Sensor Net and a Quadtrode CV (Invivo, Orlando, FL, USA) for ECG recording. The electrode at position C_z was used as reference during recording. Sampling rate was 1000 Hz because lower sampling rates result in aliasing in the scan-pulse artifact, which makes proper correction impossible when recordings of EEG and fMRI are not synchronized.

2.3.2. EEG preprocessing

Before preprocessing, the EEG was visually inspected and channels with increased impedance and permanent artifacts were discarded from further analysis. When EEG and BOLD-fMRI are recorded simultaneously inside the MR scanner, the EEG signal is corrupted by two kinds of artifacts, the gradient artifact (Allen et al., 2000; 1998) and the ballistocardiogram (BCG) (Christov, 2004; Niazy et al., 2005; 1999). To remove them, the EEGs acquired inside the MR scanner were post-processed with the average artifact subtraction method of the FMRIB plug-in (https://fsl.fmrib.ox.ac.uk/eeglab/fmribplugin/) for EEGLAB (https://sccn.ucsd.edu/eeglab/index.php, Delorme and Makeig, 2004; Iannetti et al., 2005; Niazy et al., 2005) including fitting and subtraction of optimal basis functions (OBS) derived from the first three principal components of the artifact residuals. Then a 4th-order Butterworth low pass filter was applied with a cut-off frequency at 40 Hz. The filtered EEG was down-sampled to 250 Hz and the reference was recomputed to the median of all artifact free channels in order to minimize deformations of the functional network (Rios et al., 2019). Finally, the EEG recordings were filtered in the range of 0.5 Hz - 25 Hz in order to diminish the influence of physiological noise and possible muscle artifacts (Whitham et al., 2007). More recently alternative approaches to EEG artifact reduction in simultaneous EEG-fMRI measurements have been proposed in Abreu et al. (2018), Mayeli et al. (2021).

2.3.3. EEG predictor

To estimate the stationary correlation pattern (Müller et al., 2014; Olguín-Rodríguez et al., 2018) we calculated the temporal, zero-lag cross-correlation matrix of the preprocessed EEG signals by a running time window with zero overlap, corresponding to the acquisition periods of the nth functional volume (duration 1980 ms) of the BOLD-fMRI sequence yielding $T = 495$ EEG samples per window ($n = 1, \ldots, N_{vol}$). The correlation matrix represents a time-dependent functional network and is estimated by

$$C_{xy}(n) = \frac{1}{T} \sum_{t=(n-1)T+1}^{nT} \bar{X}(t) \cdot \bar{Y}(t) \tag{1}$$

where $\bar{X}$ and $\bar{Y}$ denote any pair of the N_{ch} EEG channels, that were window-wise normalized to mean zero and standard deviation one. In order to obtain the SCP we followed the procedure used in Müller et al. (2014) and calculated the mean correlation matrix

$$SCP_{xy} = \frac{1}{N_{vol}} \sum_{n=1}^{N_{vol}} C_{xy}(n)\,. \tag{2}$$

From $C(n)$ the square matrix SCP inherits the properties of having dimension N_{ch}, being real and symmetric. In addition, all diagonal elements are equal to one.

If $C_{xy}(n)$ has a nonzero value, in the limit $T \to \infty$ there is a true similarity between signals X and Y and one supposes that the brain activities generating these signals are functionally interrelated. However, for finite T, numerical estimates of $C_{xy}(n)$ also have nonzero values. The corresponding probability distribution $P(C)$ is symmetric around zero and its width increases with decreasing T. This probability distribution

depends on the frequency content of the signals X and Y, since a given T might be short for slow frequency components (T contains only a few or no complete oscillations) or long for fast activity (Müller et al., 2011). This phenomenon is called "random correlations" in the literature (Laloux et al., 1999; Plerou et al., 1999). However, due to the symmetry of $P(C)$ these contributions cancel on average. In consequence SCP_{xy} is *not* contaminated by random effects but rather reflects stationary genuine correlations. We will come back to this issue in the discussion section.

Similarities between two matrices A and B were estimated by

$$sim(A,B) = \frac{2}{N_{ch}(N_{ch}-1)} \sum_{y>x} \tilde{A}_{xy} \cdot \tilde{B}_{xy} \tag{3}$$

where the tilde denotes normalization of the upper triangular elements to zero mean and unit variance. Due to this normalization, this similarity measure is insensitive to the variance or constant offsets of the matrix elements and purely quantifies the topological similarity between the matrices. As *EEG predictor* for the BOLD signal we estimated the *temporal similarity* (ts) between the EEG correlation matrix $C(n)$ of Eq. (1) and the SCP matrix of Eq. (2):

$$ts(n) = sim(C(n), SCP) \tag{4}$$

2.4. Relating EEG and BOLD networks

2.4.1. General linear model

By means of the General Linear Model (GLM), we studied the relationship between temporal variations of the EEG network (i.e. the temporal similarity measure $ts(n)$ of Eq. (4) after convolution with the hemodynamic response function (HRF)) and the BOLD signals. The statistical analysis was carried out using FSL's FILM with local auto-correlation correction (Woolrich et al., 2001). The design matrix of the GLM was composed of 28 variables, the EEG predictor and 27 confounding variables. The confounding variables were: the 6 motion parameters (3 translation and 3 rotation variables, output of MCFLIRT Friston et al., 1996), their 6 discrete temporal derivatives, their 6 squares and the 6 discrete temporal derivatives of the squares, yielding a total of 24 confounding variables altogether. Finally, we added the mean signals of the white matter (WM) and the cerebro-spinal fluid (CSF) as well as the discrete temporal derivative of the EEG predictor. The EEG predictor and it's derivative were convolved with the HRF modeled by a double gamma variate. To calculate the contrast of our analysis, only the predictor of Eq. (4) was given weight one, whereas the 27 confounding variables were given zero weights.

The group analysis was performed by a multi-subject GLM, corrected for multiple comparisons using FSL's randomise algorithm, a non parametric permutation inference tool (Beckmann et al., 2003; Woolrich, 2008; Woolrich et al., 2004) with 5000 permutations thresholded at $Z \geq 3.1$ and a cluster-corrected significance threshold of $P \leq .05$ (Worsley, 2001).

2.4.2. Independent component analysis

For later comparison of the statistical maps obtained by the GLM, we also assessed the resting-state networks (RSN) of the BOLD signals by means of a spatial independent component analysis (ICA). We used probabilistic ICA (Beckmann and Smith, 2004) as implemented in MELODIC (multivariate exploratory linear decomposition into independent components) Version 3.15, part of FSL. By eye inspection, we determined that 25 RSN's represented a better separation between the most reported functional networks. So, after preprocessing (masking of non-brain voxels with FSL-BET, normalizing voxel time series to zero mean and unit variance, whitening and projection into a 25-dimensional subspace using PCA, the pre-selected choice of spatial components), the observations were decomposed into sets of vectors which describe signal variation across the temporal domain (time-courses) and across the spatial domain (maps). This was achieved by optimising for non-Gaussian spatial source distributions using a fixed-point iteration technique (Hyvarinen, 1999). The time-courses were not used in this work and the spatial maps were divided by the standard deviation of the residual noise (Beckmann and Smith, 2004; 2005) in order to obtain normalized z-score maps. Like the GLM maps the ICA maps are displayed at threshold $Z \geq 3.1$. For group ICA we concatenated the fMRI data of all patients in time dimension.

2.4.3. Comparing statistical maps derived by GLM and ICA

In order to quantify the similarity between the statistical maps obtained by the GLM based on the EEG predictor and the RSNs derived from ICA, we calculated the voxel-wise true and false positives and negatives of the positive and negative activations of GLM coinciding with a chosen ICA map. For GLM and ICA maps the same threshold $Z \geq 3.1$ was chosen. From the confusion matrices we calculated the diagnostic odds ratio (DOR) (Glas et al., 2003) and Matthews Correlation Coefficient (MCC) (Chicco et al., 2021) as accuracy quantifiers that are known to show only weak dependence on the prevalence of activated voxels, i.e. the class imbalance. As secondary (but prevalence dependent) accuracy quantifiers we also report sensitivities (also known as recall) and specificities as well as positive predictive values (PPV, also known as precision) and negative predictive values (NPV).

Sensitivity (specificity) quantifies the fraction of voxels inside (outside) the RSN map of the ICA (i.e. the "target") that are activated (non-activated) by the GLM (i.e. the "prediction"). Conversely, PPV (NPV) is the fraction of all activated (non-activated) GLM voxels that fall inside (outside) the RSN map of the ICA. All these quantifiers fall in the interval $[0, 1]$. For example, PPV ≈ 1 means that almost all voxels activated by the GLM belong to a particular RSN. The DOR measures the effectiveness with which GLM activations determine the RSN by taking the ratio of the odds of a voxel being activated if it is part of the RSN relative to the odds of being activated if it is not part of the RSN. Values are between zero and infinity and only DOR $\gg 1$ represent useful agreement between prediction and target. MCC is the Matthews correlation between binary GLM activation and binary RSN membership. It ranges between -1 and $+1$.

2.4.4. Statistical evaluation

The original group analysis consisted of 53 single-subject statistical maps due to a personal EEG predictor, see Section 2.4.1. To rule out stochastic effects on our analysis of combined EEG and BOLD-fMRI data (see below) we applied three tests. Two of them were based on different kinds of surrogate predictor time series and the third on a permutation test. For each test, we generated six surrogate predictors, meaning that for each test 318 single subject analyses were performed altogether. This choice represented a compromise between numerical precision and computational effort.

Test 1, Shuffle Surrogates: We used random shuffles of the original EEG predictors to test the null hypothesis that the statistical maps obtained by EEG predictors is different from *uncorrelated noise*. This test preserves the amplitude distribution of the original EEG predictors and allows to document the existence of temporal structure in the BOLD response to our EEG predictors.

Test 2, IAAFT Surrogates: In order to disprove spurious activation due to *auto-correlated noise* (e.g. large power in low frequencies), iterative amplitude-adjusted Fourier transform (IAAFT) (Lancaster et al., 2018; Schreiber and Schmitz, 1996; 2000) surrogates of the EEG predictors were generated, conserving the amplitude distribution and the power spectrum of the original predictors while randomizing the Fourier phases.

Test 3, Permutation Surrogates: Finally, we generated six random permutations of the patients' EEG predictors, viz. estimating the BOLD activation of one patient due to the EEG predictor of a randomly chosen other subject avoiding repetitions.

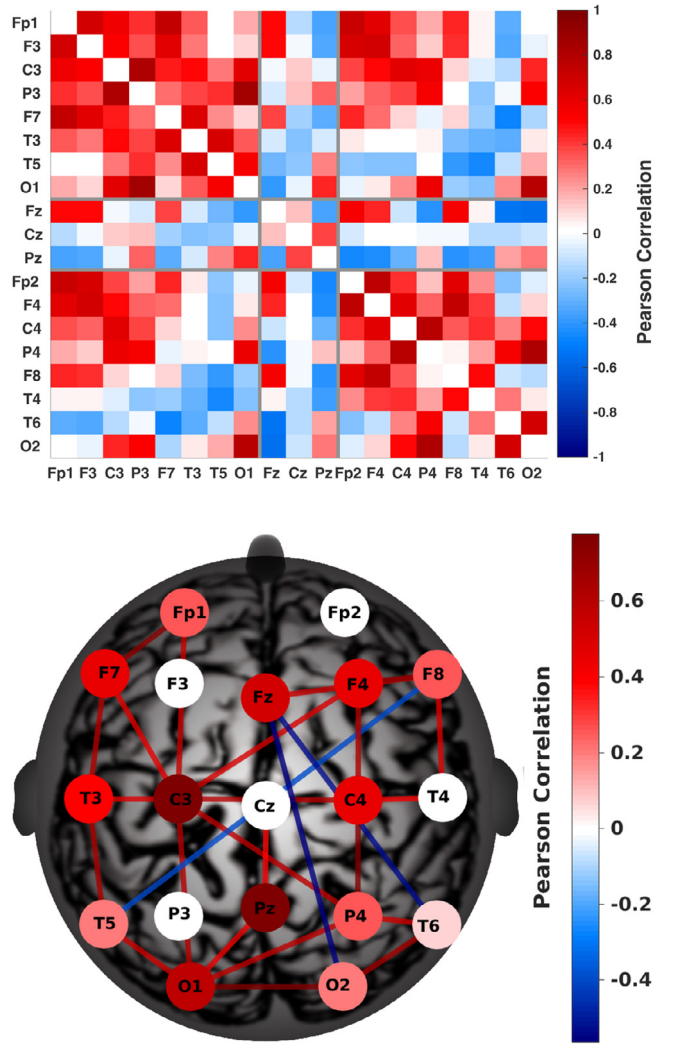

Fig. 1. *Stationary Correlation Pattern of broad-band EEG*. In panel (a) the SCP of patient A_{08} is displayed in matrix form and in panel (b) in network form. The diagonal elements of the matrix representation were set to zero manually to improve visibility. Network nodes are given by the electrode locations and links represent the association strength SCP_{xy} between node pairs. We assumed that a "distance" d_{xy} between two signals X and Y is inversely proportional to the absolute value of the association, i.e. $d_{xy} = 1/|SCP_{xy}|$ and calculated the "betweeness" as the percentage of shortest paths crossing a particular node ("node betweeness") or link ("edge-betweeness"). To increase clarity of the network representation, only 15% of the edges are displayed according to largest edge betweeness. Network nodes and edges are represented by the same color scale. The edge color indicates the value of the matrix element SCP_{xy}, whereas the node color indicates the node-betweenness of the full network.

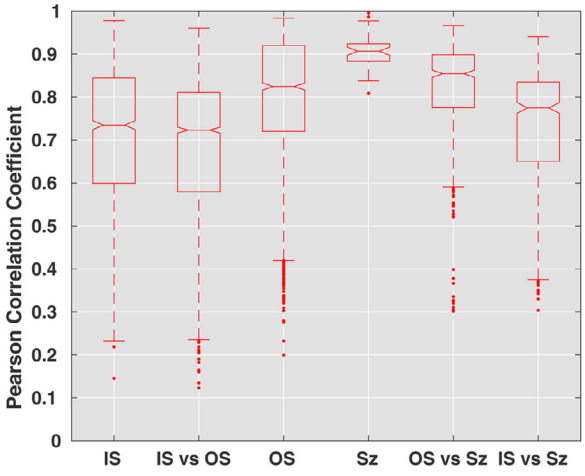

Fig. 2. *SCP universality - distribution of matrix similarities.* Columns 1 to 3 show the boxplots of similarity values for the comparison of SCP obtained for different conditions. Comparison is made within all the SCP of different patients inside the scanner (IS, $53 \cdot 52/2 = 1,378$ values), inside versus outside (IS vs. OS, $53^2 = 2809$ values) and outside the scanner (OS, $53 \cdot 52/2 = 1,378$ values). The 4th column (group "Sz") corresponds to the SCP of epilepsy patients ($10 \cdot 9/2 = 45$ comparisons) from Müller et al. (2014) and columns 5 and 6 make direct comparison with our recordings outside and inside the MR scanner ($10 \cdot 53 = 530$ comparisons each).

3. Results

3.1. EEG network and predictor

In this work we concentrate on reporting results for the EEG predictor calculated from the 19 electrodes of the 10–20 EEG system and broad-band filtering.

Fig. 1 a shows the SCP matrix of patient A_{08} calculated according to Eq. (2) and Fig. 1b displays its network representation. In this single patient recording the interrelation pattern found in Müller et al. (2014) is confirmed apart from the difference that a slightly altered electrode configuration was used (19 instead of 15 electrodes, see Section 1.2 of supplementary materials for EEG configuration details).

To assess the influence of scanner artifacts on the SCP also on the group level we calculated SCP matrices of Eq. (2) from all EEG recordings outside and inside the scanner (two times 53 matrices altogether). For direct comparison with Müller et al. (2014), the pairwise matrix similarities Eq. (3) for the 15-electrode configuration are displayed as boxplots in Fig. 2 (corresponding cumulative density functions for the 19-electrode configuration are provided in the Supplementary Materials). Compared to matrix similarities between the SCPs of EEGs recorded outside the scanner, those recorded inside the scanner are shifted towards smaller values even after the pre-processing. However, in general we observe a high similarity in all cases (only 10% have a correlation coefficient smaller than 0.5) and the null hypothesis of vanishing similarity can be rejected with high certitude. The SCPs calculated from EEGs recorded inside and outside the MR scanner were also very similar to those obtained in previous studies (Müller et al., 2014) under different experimental as well as physiological conditions, see last two columns of Fig. 2. We conclude that despite scanner effects the generic SCP is still clearly identifiable after pre-processing also on the group level.

The temporal evolution of the elements of the cross-correlation matrix Eq. (1) and the EEG predictor Eq. (4) of patient A_{08} and broad-band filtering are displayed in Fig. 3, illustrating the high stability of the correlation pattern over time. The EEG predictor $ts(n)$ of Eq. (4) fluctuates mainly between 0.8 and 0.95 and never drops below 0.55, a value that still indicates a very close match between the temporal correlation matrix $C(n)$ and the stationary pattern SCP. Fluctuations of the spatial correlation structure remain small and matrix elements almost never change sign, such that the overall topology of the correlation matrix is almost always conserved over the whole time course. Rearrangements of the correlation matrix between minute 1 and 2 as well as around 8 and 14 min after the start of the recording (top panel) are well reflected by transient drops of the EEG predictor (bottom panel), indicating a reduced agreement with the SCP displayed in Fig. 1. Note, however, that the overall pattern of the SCP is still clearly recognizable even in these periods, see Fig. S3 of the Supplementary Materials.

The EEG predictor derived from the 19 electrodes of the 10–20 system was compared to analog definitions calculated from different electrode selections. First, to exclude the potential influence of artifacts due

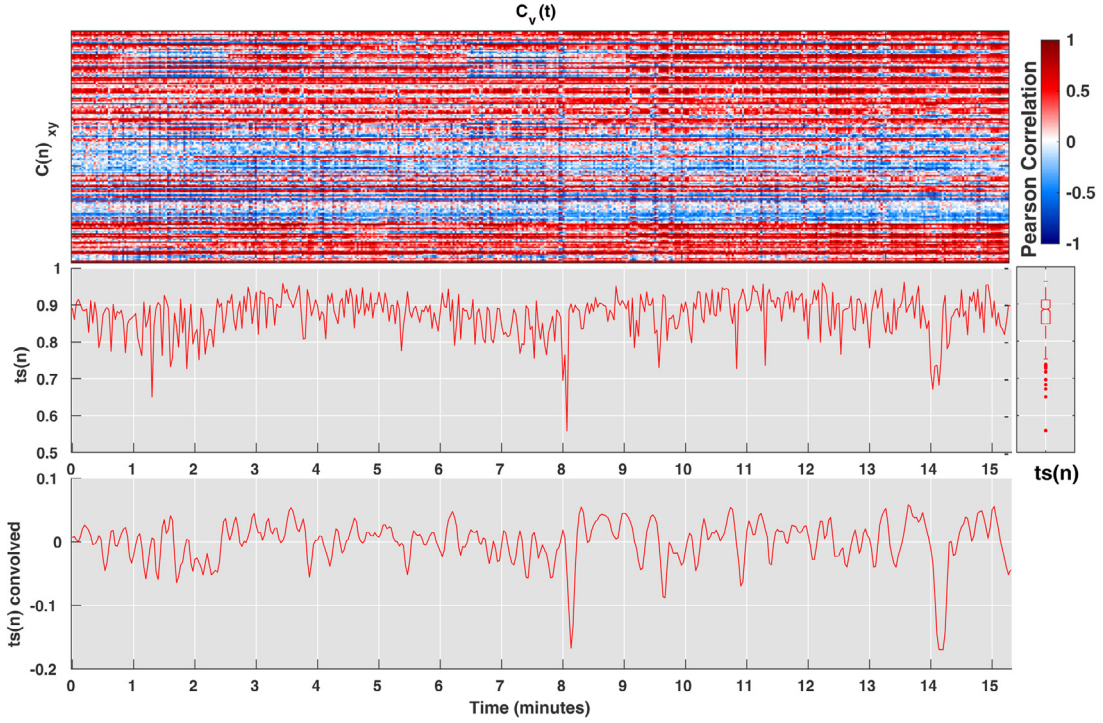

Fig. 3. *Temporal evolution of the correlation pattern in broadband EEG.* The top panel shows the vectorized correlation matrix $C_{xy}(n)$ of patient A_{08} over the 460 time windows, the color bar indicating the value of the matrix elements. The middle panel displays the EEG predictor defined in Eq. (4), whereas the bottom panel shows its shape after whitening and convolution with the HRF.

to eye and head movements, we restricted the analysis to the 15 electrodes of the 10–20 system excluding positions Fp_1, Fp_2, O_1 and O_2. In addition we studied the EEG predictor calculated from the EEG signals recorded at all 255 electrodes of the Geodesic cap (except C_z, which was used as recording reference). The Pearson correlation between the EEG predictors of these three electrode configurations was generally high, see Fig. S1 of the Supplementary Materials for the 19-electrode configuration. For patient A_{08} the values were $r_{(15,19)} = 0.95$, $r_{(15,255)} = 0.81$ and $r_{(19,255)} = 0.85$. The densely packed EEG sensors of the Geodesic cap record redundant brain signal information on neighboring electrodes, which in turn leads to excessively high estimates for the correlation coefficient. This justifies restriction of the presentation of our results to the SCP derived from the subset of 19 electrodes used in the international 10/20 system.

3.2. GLM analysis

Statistical maps of the single-subject GLM analysis of patient A_{08} based on the broad-band EEG predictor are shown in Fig. 4 as Z-score maps. Using the same threshold $Z \geq 3.1$ the positive GLM activation (red) is almost completely located inside the ICA map corresponding to the DMN identified in the same subject.

Fig. 5 shows the group-wide statistical maps, denoted as positive and negative activation in relation to a positive or negative contrast of the EEG-predictor. We observed positive activation in precuneus, medial frontal and inferior parietal and temporal regions. Negative activation includes temporal and insular regions as well as parts of the anterior cingulate. A complete report of the positive and negative activation regions according to the Anatomical Automatic Labeling (AAL) atlas (Tzourio-Mazoyer et al., 2002) is compiled in Tables S2 and S3 of the Supplementary Materials.

The statistical maps of surrogate tests are shown in Fig. 6. The top panel displays the (positive) activation for the three surrogate-based tests in different colors. Negative activation provoked by the same surrogate predictor is shown at the bottom panel. When displaying these

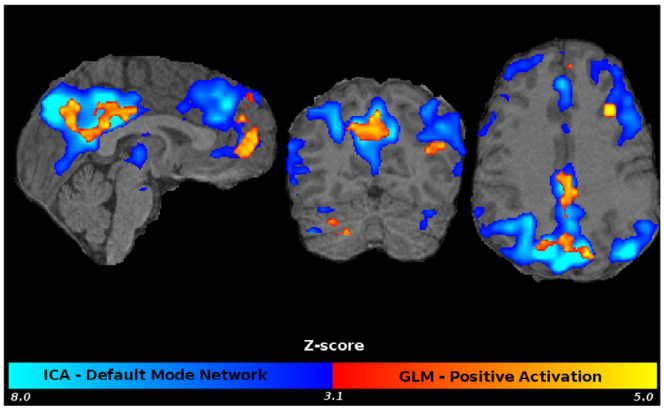

Fig. 4. *Single-subject maps of GLM and ICA for patient A_{08}.* Both statistical maps were thresholded at $Z \geq 3.1$ and are displayed in neurological orientation (i.e. the left hemisphere appears on the left of the image).

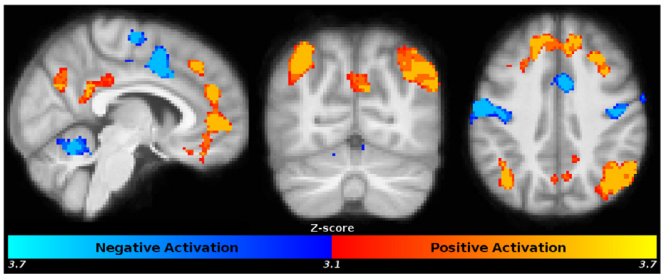

Fig. 5. *Group statistical maps for the EEG predictor.* Positive activation (red) and negative activation (blue) of group GLM analysis are displayed in neurological orientation after thresholding at $Z \geq 3.1$. Coordinates: X=6 | Y=-67 | Z=38. (For interpretation of the references to colour in this figure legend, the reader is referred to the web version of this article.)

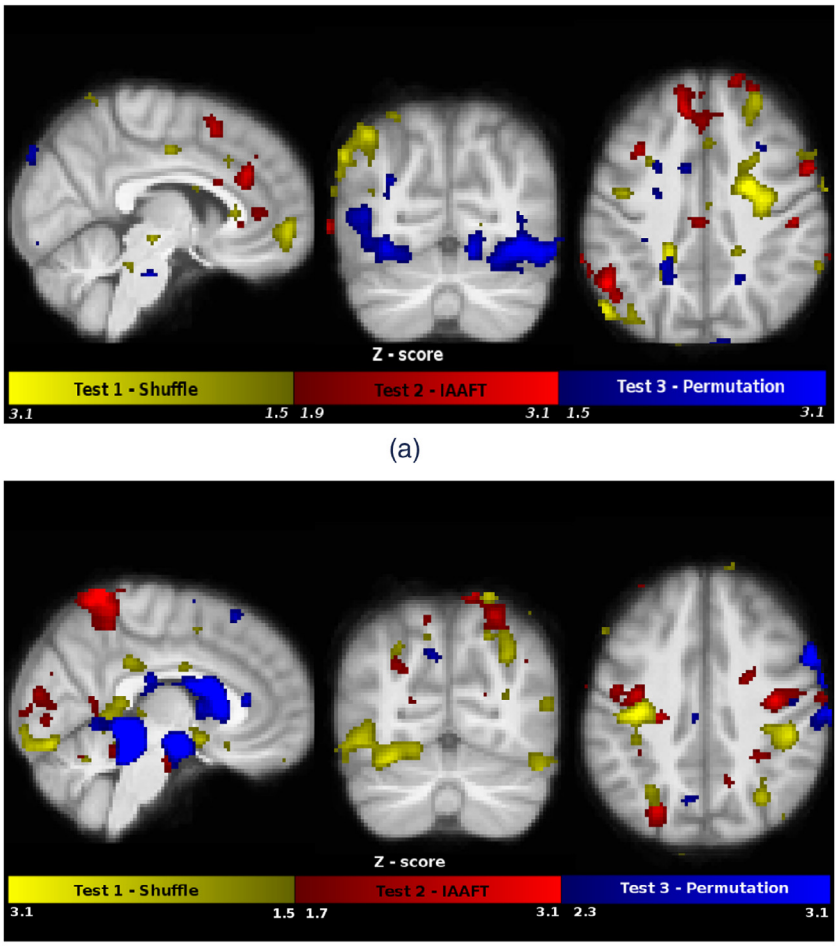

Fig. 6. *Statistical maps for group analysis of surrogate predictors.* All the panels were thresholded at substantially lower Z values than in Fig. 5 to yield the same number of activated brain voxels (i.e. 9748 positively and 7721 negatively activated voxels). For positive activation (panel a) the threshold was set at Z≥1.5 for the shuffle surrogates (yellow), at Z≥1.9 for IAAFT surrogates (red), and at Z≥1.5 for the permutation surrogates (blue). For negative activation (panel b) the threshold was set at Z≥1.5 for the shuffle surrogates (yellow), at Z≥1.7 for IAAFT surrogates (red), and at Z≥2.3 for the permutation surrogates (blue). Images are shown in neurological orientation. Coordinates: X=6|Y=-67|Z=38. (For interpretation of the references to colour in this figure legend, the reader is referred to the web version of this article.)

maps using the same threshold as in Fig. 5 no significant voxels were observed. In order to achieve the same number of activated voxels as for the positive and negative activation due to the original predictor (9748 and 7721 at Z≥3.1) Z-values were notably reduced. After this reduction the activation patterns appear incoherent and do not resemble any of the known RSN maps.

3.3. Comparison: GLM vs. ICA

Eleven RSNs were identified by visual inspection of the group ICA results, among them the default mode network (DMN) (Greicius et al., 2003; Raichle et al., 2001), the salience network (SN) (Menon and Uddin, 2010) and the executive control network (ECN) (Seeley et al., 2007). Quantifiers for agreement of positive and negative activations of the broad-band EEG predictor with the eleven RSNs are compiled in Tables 1 and 2. The strongest agreement (highest DOR) of positive activation to the EEG predictor was found for the DMN and superior part of the ECN. Negative activation agreed strongest with SN.

A group comparison of the positive activations of the EEG-predictor with RSN01 (resembling the superior part of the ECN) and RSN02 (resembling the DMN) is provided in Fig. 7a. The same comparison between negative activations of the EEG predictor and RSN04 (resembling the SN) is displayed in Fig. 7b. Like in the case of the single subject analysis (Fig. 4 we observe that the GLM-maps fell almost completely inside the statistical maps obtained by ICA and only a small percentage of the activated voxels was outside the ICA-RSN.

This visual impression is quantitatively confirmed by different accuracy quantifiers provided in Tables 1 and 2. A general observation is that specificities and NPVs were close to one, indicating that the number of true negative voxels was much larger than the numbers of false positives and negatives, respectively. In contrast, PPVs and sensitivities of RSN01, RSN02 and RSN04 were only moderate or even low, indicating that the number of true positive voxels was comparable to or even smaller than the number of false positives and negatives, respectively. Positive and negative GLM activations of the EEG predictor were most

Table 1
Agreement between the group statistical maps of positive GLM activations of the EEG predictor and RSNs derived from ICA. Abbreviations: RSN, resting state network; DOR, diagnostic odds ratio; MCC, Matthew's correlation coefficient; Sens., sensitivity; Spec., specificity; PPV, positive predictive value; NPV, negative predictive value.

RSN	DOR	MCC	Sens.	Spec.	PPV	NPV
1	5.203	0.174	0.137	0.97	0.39	0.891
2	9.323	0.249	0.208	0.973	0.413	0.93
3	1.67	0.041	0.064	0.961	0.199	0.871
4	0.123	-0.066	0.006	0.952	0.017	0.877
5	1.987	0.049	0.076	0.96	0.145	0.922
6	3.27	0.082	0.117	0.961	0.131	0.956
7	1.496	0.029	0.06	0.959	0.147	0.897
8	0.628	-0.023	0.028	0.956	0.059	0.908
9	0.081	-0.065	0.004	0.953	0.01	0.892
10	0.133	-0.05	0.006	0.955	0.01	0.927
11	0.05	-0.052	0.002	0.955	0.004	0.933

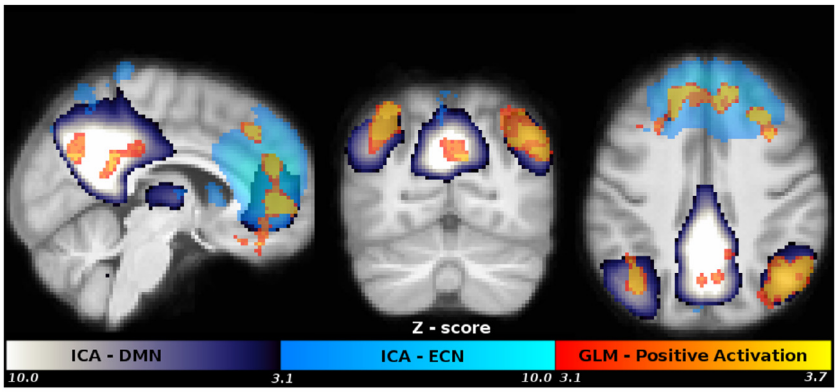

(a)

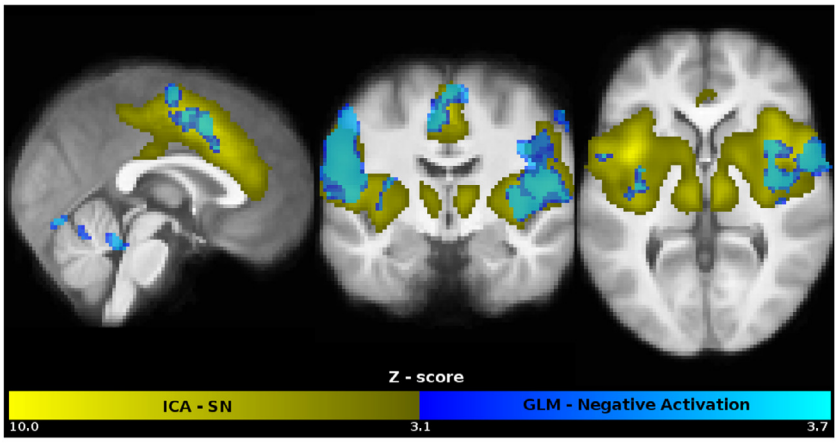

(b)

Fig. 7. *Statistical maps of group GLM and group ICA.* Panel **(a)** shows the maps for the DMN (blue-white) and ECN_s (cyan) obtained by ICA, and the positive activation map obtained by the EEG-predictor (red-yellow, same data as shown in Fig. 5). Coordinates: X=6|Y=-67|Z=38. Panel **(b)** shows the SN (yellow) obtained by ICA and the negative activation map obtained by the EEG predictor (blue-cyan). Coordinates: X=0|Y=-7|Z=2. All panels are shown in neurological orientation and thresholded at $Z \geq 3.1$. (For interpretation of the references to colour in this figure legend, the reader is referred to the web version of this article.)

Table 2
Agreement between the group statistical maps of negative GLM activations of the EEG predictor and RSNs derived from ICA. Abbreviations: RSN, resting state network; DOR, diagnostic odds ratio; MCC, Matthew's correlation coefficient; Sens., sensitivity; Spec., specificity; PPV, positive predictive value; NPV, negative predictive value.

RSN	DOR	MCC	Sens.	Spec.	PPV	NPV
1	0.083	-0.063	0.003	0.962	0.012	0.875
2	0.013	-0.056	0.001	0.963	0.001	0.912
3	0.234	-0.053	0.009	0.962	0.035	0.864
4	31.91	0.378	0.22	0.991	0.772	0.904
5	1.196	0.009	0.04	0.967	0.095	0.919
6	0.002	-0.042	0	0.965	0	0.951
7	1.971	0.048	0.059	0.969	0.184	0.898
8	3.075	0.087	0.084	0.971	0.223	0.914
9	1.892	0.044	0.057	0.969	0.176	0.899
10	0.262	-0.037	0.01	0.964	0.02	0.928
11	0	-0.049	0	0.964	0	0.933

often found inside the RSNs but only rarely outside. They represent only core regions of the RSN templates, not their entirety.

4. Discussion

Using simultaneous EEG-fMRI recordings from 53 epilepsy patients, we found that the cross-correlation structure of resting-state EEG recordings is remarkably stable over time, and that its temporal fluctuations correlate with those of known RSN derived from fMRI. Our analyses suggest that there is a core dynamical structure of large-scale brain networks that can be reliably recovered across multiple spatial and temporal scales.

The strategy of the numerical analysis was based on previous findings in EEG data, where the stationary correlation pattern has already been reported (Müller et al., 2014; Olguín-Rodríguez et al., 2018). This extremely stable, pronounced correlation structure proved independent from the physiological state and generic in the sense that very similar average patterns have been encountered across subjects and in all classic EEG bands. Here we could show that the same pattern can be identified in simultaneous EEG-fMRI after removal of scanner related artifacts on the EEG.

Dynamical aspects are reflected by tiny transient deviations from the SCP, see e.g. Fig. 3 and reference (Olguín-Rodríguez et al., 2018). On the other hand, also RSN identified by fMRI studies, represent templates for brain dynamics (Raichle, 2006). Their mutual synchrony is highly non-stationary and subject to changing cognitive processes like introspection or externally oriented tasks (Benedek et al., 2014a; Ellamil et al., 2012; Fink et al., 2009; de Manzano and Ullén, 2012). The fact that also in fMRI experiments it was found that activity during rest and task orientated activation pattern closely match and that even during rest a multitude of different RSN's are continuously active (Smith et al., 2009) constitutes a first hint that both phenomena are closely connected.

Based on these findings we have used network features of fast neuronal activity captured by EEG measurements in order to predict RSN as assessed by slow metabolic resting state activity. Specifically, we tested the hypothesis that fluctuations (see Eq. (4)) around the SCP of Eq. (2) should generate activation maps similar to RSNs when used as a predictor for the BOLD signal. So far, the vast majority of studies of simultaneous EEG-fMRI have concentrated on fluctuations of spectral power in different frequency bands (Britz et al., 2010; Goldman et al.,

2002; Horovitz et al., 2008; Jann et al., 2010; Laufs et al., 2003; Mantini et al., 2007; Neuner et al., 2014; Prestel et al., 2018; Rajkumar et al., 2018; Samogin et al., 2019), which is a univariate property and does in general not directly reflect interrelations between different brain regions.

Relative changes of the spectral power may influence our correlation-based predictor only indirectly through so-called "random correlations" (Laloux et al., 1999; Plerou et al., 1999) caused by the finite size of the data window used for the numerical estimate. High power in slow frequencies enhance random correlations (Müller et al., 2011; Rummel et al., 2010). Given that their distribution is symmetric around zero, they cancel when averaging over long data segments, which has been used to construct a genuine cross-correlation matrix (García et al. (2013)). In consequence, the pattern of the SCP defined in Eq. (2) is not affected by random correlations, but estimates taken over short time windows like the predictor defined in Eq. (4) can be. It does not only account for interrelations between signals but may carry information about relative changes of their power distribution as well – although in an indirect fashion.

It was previously shown that slow modulations (below 0.1 Hz) of respiration as well as the heart rate variability correlate notably with EEG power in the α-band (Chen et al., 2020; Yuan et al., 2013). This effect is even more pronounced at rest with closed eyes. Hence, using univariate measures like EEG power might be biased by physiological fluctuations, which in turn may distort the prediction of RSN via the GLM. In contrast, the approach proposed here is based on network properties derived from interrelations *between* EEG time series (Jann et al., 2009; Jann et al., 2008; Wiest et al., 2013) and thus presents a new perspective to link network activities acting on very different time scales. In addition, slow wave EEG activity has been eliminated by an appropriate high pass filter with cut-off frequency 0.5 Hz before further analysis.

Despite analyzing simultaneous EEG-fMRI recordings in patients with epilepsy, the present study does not make any statements about the nature of this disorder. Our justification to answer our general research question using patient data is that previous studies have found large similarities between the SCP derived from scalp EEGs of epilepsy patients and healthy subjects, regardless of analyzing preictal, ictal or postictal EEG or different physiological states like e.g. sleep stages (Müller et al., 2014; Olguín-Rodríguez et al., 2018). To observe potential differences we expect to require larger and more homogeneous groups than available for our study as well as EEG-fMRI recordings from healthy subjects.

However, even when the SCP derived from EEG is not affected by the epileptic pathology, it was shown that RSN derived from fMRI signals do undergo specific deformations (Centeno and Carmichael, 2014; Gotman, 2008; Pittau et al., 2012; Zang et al., 2012). This finding might explain the low sensitivities reported above. Hence, conducting a similar study with a sufficiently large cohort of healthy subjects would be highly desirable to investigate generic and condition specific aspects further.

4.1. EEG predictor vs. ICA

Statistical maps obtained by the EEG-predictor almost always fell inside the maps of RSNs derived from spatial ICA of BOLD-fMRI data and only small regions were located outside, see Figs. 4 and 7 for results on the single-subject and group levels, respectively. In particular, highest agreement of positive activations was observed for the ECN (RSN01, DOR>5) and the DMN (RSN02, DOR>9), whereas negative activation was strongly associated with the SN (RSN04, DOR>31), see Tables 1 and 2. In particular, for negative activation and the SN a PPV = 0.77 was found, meaning that 77% of the voxels that showed significant negative activation in response to the EEG predictor were indeed also associated with negative correlates of the SN. For positive activation the corresponding fraction was 39 and 41% for the ECN and DMN, respectively.

Across all RSNs we observed high specificities and NPV, whereas sensitivities and PPV were only moderate or even low. High specificities and NPVs are explained by low prevalence, i.e. the large number of brain voxels compared to the number of voxels involved in GLM activations and RSN maps. In consequence, the number of false positives and negatives was small compared to the large number of true negatives. PPVs were in general larger than sensitivities, sometimes much larger. This is explained by a smaller number of false positives than false negatives, meaning that more voxels inside the RSN maps are missed than activated outside the RSNs in response to the EEG predictor.

We contrasted these results by the activations in response to three different methods to generate surrogate predictors representing the null hypothesis that the findings occurred by chance. For all types of surrogates we obtained sub-threshold, randomly distributed and mutually inconsistent activation maps covering the whole brain, which did not coincide with any of the known RSNs.

The EEG-predictor was derived from an extra-cranial measurement at large distance from the system generating the signals and with several perturbing layers in between (skin and muscles, cranium and cerebrospinal fluid), which act as a temporal low-pass filter and diminish the signal to noise ratio. However, this measurement is used for the modeling of activity even deep inside the brain. Hence, it is conceivable that regions with slightly less intense power are hardly modeled by distant surface estimates of fast processes. Therefore, we expected in advance rather low sensitivity values (i.e. a considerable amount of false negatives) for our procedures, like those reported in Tables 1 and 2.

An additional reason for the notably low sensitivity values observed by us might be due to the influence of physiological noise provoked by slow modulation of respiration variations and heart rate changes in a range below 0.1 Hz. Even after applying correction schemes described in the method section, the fMRI-recordings might carry the influence of slow physiological fluctuations, given that such activity shows a certain similarity with the neural activity of RSN (Chen et al., 2020).

By such a mechanism the ICA-estimations might become enlarged, in turn reducing the sensitivity values of the GLM predictor.

4.2. Interrelation between networks

We found that deviations from the SCP correlate with key-nodes of the DMN. This is in keeping with the DMN's prominent role during resting-state experiments. It is supposed to be active during self generated thoughts and *internally* directed cognition, such as mind wandering (Mason et al., 2007), future thinking (Schacter et al., 2012) or mental simulation (Buckner and Carroll, 2007), but it was also shown that the DMN is engaged during creative assignments (Benedek et al., 2014b; Fink et al., 2009; McMillan et al., 2013). To all these processes different nodes of the DMN may contribute in different proportion; for instance, the precuneus during divergent thinking (Benedek et al., 2014a; Fink et al., 2014; Takeuchi et al., 2011), while the inferior parietal lobule during linguistic exercises (Fink et al., 2009), the left inferior parietal cortex when generating creative uses for given common objects (Benedek et al., 2014b).

Contrary to that, the ECN is engaged in *externally* directed tasks that require working memory (Curtis and D'Esposito, 2003), memory encoding (Blumenfeld et al., 2011), response inhibition (Aron, 2007), or cognitive control processes (Dreher and Berman, 2002) but was also shown to be active during divergent thinking (Beaty et al., 2015) or other creative demands like musical improvisation as well as drawing (Ellamil et al., 2012).

Consequently, it is thought that DMN and ECN act in opposition to each other, such that when one network increases activity the other one diminishes power (Fox et al., 2005; 2009). The alternate activity pattern of both large scale networks seems to be mainly moderated by the right anterior insula, a core region of the SN (Menon, 2011; Menon and Uddin, 2010), which is supposed to be responsible for the orientation of attention (Bressler and Menon, 2010; Goulden et al., 2014; Menon and Uddin, 2010; Sridharan et al., 2008).

At the first glance, our results seem contradictory given that we found a simultaneous positive activation in parts of the DMN and ECN,

whereas parts of the SN showed significant negative activation in response to our EEG derived predictor. However, the purely modular perspective that DMN and ECN should always be anti-correlated due to apparently different, specific duties they have to fulfill, is possibly too rigid and does not account for the high flexibility of brain dynamics. Even neuronal populations of primary sensory areas of the cortex have been shown to be cross-modular (Ghazanfar and Schroeder, 2006) and the idea that different brain areas are responsible for the execution of specific tasks, which are accomplished almost independently from others, is probably not quite realistic (Fuster, 2000). By using graph theoretical techniques it was explicitly shown in Beaty et al. (2015) that the DMN correlates with the ECN as well as with the SN, but during different episodes of task performance.

Since the brain permanently generates the maximal possible number of space-time patterns (see Section 4.3), also brain networks should support and contribute to this diversity (Sporns and Kötter, 2004). In consequence, it is conceivable that different areas of a network contribute with different strength to distinct tasks (see e.g. Bressler and Menon, 2010; Preti et al., 2017) and references therein). Furthermore, it has been suggested that different frequency bands of the electrical brain activity measured by EEG are related to different areas of resting state networks (Jann et al., 2009; Jann et al., 2010; Mantini et al., 2007; Samogin et al., 2019).

Hence, the finding that like the DMN also the ECN is involved in various creative exercises, is a strong hint that both networks may also cooperate in order to fulfill certain demands, viz. they may synchronize as observed by us. The simultaneous positive activation of voxels in parts of DMN and superior ECN in the present study is probably related to mind wandering, in particular unaware mind wandering (Christoff et al., 2009) and could be related to future thinking and creativity (Beaty et al., 2015). So far, we succeeded to prove that fluctuations around the SCP serve well as a predictor for RSN. But it remains an open question, whether this is just an incidental finding linking phenomena operating on very different time scales, or, whether the SCP has a deeper physiological meaning. In the next two sections we discuss a possible interpretation of the SCP. Considering physical systems that would lead to observations like the SCP, we relate it to more established theoretical frameworks.

4.3. Complexity and criticality

Thermodynamic systems at (or close to) the critical point of a second order phase transition (Chialvo, 2007; Chialvo, 2010; Cocchi et al., 2017; Fraiman et al., 2009) produce the largest possible set of different spatio-temporal structures. This is expressed by power law distributions, which implies that the system is scale free, meaning that it does not account for a typical scale (in whatever units) (Kello et al., 2010). This maximal variability is by far not amorphous, but regulated by strong correlations of maximal length, spanning over the entire system.

These characteristics for the vicinity of critical points - a huge variety of different space-time patterns and power law distributions as well as far-reaching stable correlations like the ones observed in this work - are indeed observed in brain dynamics: Even at rest the brain is never resting but permanently active (Fox and Raichle, 2007; Raichle, 2006; Raichle, 2011; Smith et al., 2009) and this resting state activity is by far not erratic. It is well established that goal directed tasks require specific spatio-temporally synchronized neural activity (Singer (1993)). However, also at rest brain dynamics spontaneously creates transient synchrony in neural populations before these patterns decay or provoke avalanches of synchronization (Beggs and Plenz, 2003; Cocchi et al., 2017; Linkenkaer-Hansen et al., 2001; Palva et al., 2013; Tagliazucchi and Chialvo, 2011; Yang et al., 2012). The size as well as lifetime distribution of synchronized patterns follows with high precision power laws (Fraiman et al., 2009; Tagliazucchi et al., 2012), which implies that the brain creates continuously the maximal possible set of synchronized space-time structures, a behavior that is substantiated by empirical data in both in-vitro (Beggs and Plenz, 2003; Beggs and Timme, 2012) as well as in-vivo experiments (Petermann et al., 2009), by means of fMRI, MEG and EEG measurements (Fraiman et al., 2009; Linkenkaer-Hansen et al., 2001; Tagliazucchi et al., 2012). This high variability at all spatial and temporal scales is contrasted by the observation of the SCP observed in EEG-recordings (Müller et al., 2014; Olguín-Rodríguez et al., 2018), which reflects strong and far-reaching correlations and is in contrast to the naive expectation of tiny average correlations between highly non-stationary and noise contaminated time series.

The strongly correlated ongoing neural activity with maximal variation of the production of space-time structures provides a compromise between excitation and inhibition in a self-organized fashion as typical for a complex adaptive system (Singer, 2013) at a critical point (Poil et al., 2012; Poil et al., 2008). The huge variability of neural activation patterns assures segregation, while integration requires strong long range correlations. At the critical point, a finely tuned balance between segregation and integration is achieved, which in turn assures a very effective information processing.

In particular, for the brain those far-reaching correlations are vitally important, because they avoid that just by chance a space-time pattern of synchronized neural activity is produced that causes undesired corporal or mental actions. This mechanism assures a robust dynamics but simultaneously allows for maximal variability (Yang et al., 2012), which is certainly required, given that the brain permanently adapts its dynamics to external stimuli as well as to ever changing internal conditions governed by (control) processes. The hierarchical organization of brain structures (Buzsaki, 2006; Vidaurre et al., 2017) substantiates this picture. In conclusion, the observation of the SCP does not imply complexity or that the brain dynamics occurs close to a critical state, but if brain is a complex system and operates close to a critical point, a pattern sharing the features of the SCP would be a consequence.

4.4. Attractor activity and transient dynamics

Inspired by previous results (Olguín-Rodríguez et al., 2018) we designed the GLM-predictor capable to detect several RSNs with high specificity. Transient dynamical features are expressed by tiny excursions from the SCP, which in turn, are reflected by slow metabolic dynamics of cortical and subcortical regions. A possible interpretation is that the SCP as well as the known RSNs constitute a dynamical scaffold like an attractor in phase space of a dynamical system (Singer, 2013), where external impulses provoke (comparably small) deviations from it. Viewing the brain as a complex dynamical system, possibly combined with a notable stochastic component, but still with pronounced phase space structure, fits precisely to our empirical findings.

This scenario is also consistent with the so called “brain’s dark energy” (Raichle, 2006), viz. the high energy consumption of the brain even at rest, which is by an order of magnitude disproportional compared to its small fraction of the whole body mass. Up to 80% of this energy is expended by neural signaling processes, while the energy increase related to a typical task-related response is in general tiny (of the order of 1%) (Raichle and Mintun, 2006). From this point of view the brain is operating autonomously, while processing of sensory information only interferes marginally. Hence, if the SCP is associated with the ongoing intrinsic activity, one should expect that task related dynamics only cause small modulations of this generic correlation structure and that in general terms the topology of the functional network should be preserved, as already reported in Müller et al. (2014), Olguín-Rodríguez et al. (2018) and confirmed in the present work.

But the brain is hardly ever moving within the set of state space vectors constituting the attractor in phase space. It is much more conceivable that this system evolves permanently with a kind of transient dynamics, because alternating internal parameters as well as external stimulation push it continuously away from attractor trajectories. However, considering the tiny influence of such variations on the energy consumption, one can expect that also the excursions from the attractor

structure remain considerably small. The overall high correlation with the SCP shown in Fig. 3 as well as model calculations on the basis of coupled dynamical systems, provided in the supplementary material of Olguín-Rodríguez et al. (2018), strongly supports this conjecture. This implies, that not the correlation estimates themselves are most convenient for the description of transient dynamics like cognitive processes or epileptic seizures, but the interesting dynamical features are probably much better encoded by deviations from it. Preliminary results presented in Olguín-Rodríguez et al. (2018) are already pointing in this direction. Hence, fluctuations around as well as deviations from average stationary structures reflect the response of the system to e.g. a visual stimulus or a cognitive task.

Pathologies, on the other hand, should then manifest themselves in deformations of the attractor in analogy to e.g. deformations of the RSN as already abundantly reported (Bressler and Menon, 2010; Menon, 2011; Pievani et al., 2011). This should also affect the SCP, meaning that, one might expect (possibly small) deformations in certain neurological disorders and further it might develop with age. Studying these questions is reserved for future research. Furthermore, the communication between RSNs could be distorted as e.g. reported in Manoliu et al. (2014), where it was found that the interaction between DMN and ECN has been significantly altered in patients with schizophrenia, in comparison to a control group. This was traced back to an aberrant activity of the anterior insula, a core node of the SN (see also Marstaller et al., 2021).

Also the transient behaviour could be distorted, viz, the system could react in an exaggerated fashion, such that fluctuations around stable structures could be excessively large, or, conversely, the system could loose sensitivity and fluctuations could be significantly diminished (Preti et al., 2017). In fMRI such findings have been already reported. In Garrett et al. (2013), Grady and Garrett (2014) it was even considered that the “moment to moment brain variability” in BOLD signals could have a predictive meaning, such that a high variability was associated with a better cognitive task performance and was found to be systematically higher in young adults in comparison with elderly subjects. These results were confirmed recently (Boylan et al., 2021; Millar et al., 2020). On the other hand, a decreased BOLD signal variability has been found in patients with Alzheimer’s disease and correlated with cognitive decline (Zhang et al., 2020). Finally, variability increased with development, which was observed in EEG (McIntosh et al., 2010) and MEG (Mišic et al., 2010). Enhancement of the brain’s dynamical repertoire expressed by an apparently noisy stochastic component was attributed to an enhanced capacity for information processing.

5. Conclusions

Based on a quantitative analysis of 53 simultaneous EEG-fMRI recordings we established a direct link between networks of fast EEG activity and slow metabolic processes at rest. Motivated by fundamental principles of dynamical systems theory we used fluctuations around a pronounced average correlation pattern of EEG-recordings as a GLM-predictor for the BOLD signal. This GLM-predictor describes RSNs derived by independent component analysis with high specificity by detecting agreement with the DMN and networks related to attention like the ECN and the SN. Furthermore, the interrelations between the SN and DMN-ECN are in agreement with previous studies (Fox et al., 2006; Fox et al., 2005; Fox et al., 2009; Hellyer et al., 2014; Menon, 2011; Menon and Uddin, 2010; Sridharan et al., 2008). We interpret these findings as possibly associated with mind wandering (Christoff et al., 2009), future thinking and creativity (Beaty et al., 2015).

The fact that tiny but permanent fluctuations around the linear SCP serve well as a GLM-predictor for RSN is congruent with the paradigm that the brain is a complex adaptive system that operates close to a critical point (Chialvo, 2007), and provides additional empirical evidence for the so called “brain’s dark energy” and the small extra energy consumption during task performance and cognition (Raichle, 2006; Raichle, 2011; Singer, 2013).

Nonlinear fluctuation properties of the signals have been considered in Portnova et al. (2018). Given the nonlinear nature of the brain dynamics, we feel that predictors derived from such nonlinear analyses could serve as promising tools for EEG-fMRI-studies that might illuminate so far unknown features.

The results of the present study imply that RSN of slow metabolic activity and the SCP found in much faster electrical brain activity as assessed by scalp EEG recordings, are just two sides of the same coin. According to the interpretation given in Olguín-Rodríguez et al. (2018) and in line with the empirical findings of the brain’s energy balance (Raichle, 2006; Raichle, 2011; Singer, 2013) it can be understood as a kind of shadow of the brain’s attractor dynamics. Then, if the attractor evolves with lifetime, the SCP could be age dependent and diseases could be expressed by possible deformations of the SCP, similar to findings in fMRI resting state networks (Bressler and Menon, 2010; Grady and Garrett, 2014; Marstaller et al., 2021; Menon, 2011; Pievani et al., 2011). Furthermore, if non-stationary dynamical features are expressed by (tiny) excursions around these stable structures, pathological behaviour could also be due to distorted fluctuation properties. In fMRI studies this hypothesis was partly confirmed (Boylan et al., 2021; Garrett et al., 2013; Grady and Garrett, 2014; Millar et al., 2020; Zhang et al., 2020), but EEG or MEG-studies pointing in this direction are still sparse (McIntosh et al., 2010; Mišic et al., 2010). We hope that the present contribution motivates future research in this spirit, acknowledging that apparently stochastic behaviour is not necessarily associated to noise components.

Data availability

We will provide anonymized and skull stripped functional and structural MRI in NIFTI format and anonymized EEG data in EDF format upon reasonable request.

Credit authorship contribution statement

J. Daniel Arzate-Mena: Methodology, Software, Visualization, Validation, Formal analysis, Investigation, Writing – original draft, Writing – review & editing. **Eugenio Abela:** Data curation, Writing – review & editing. **Paola V. Olguín-Rodríguez:** Writing – review & editing. **Wady Ríos-Herrera:** Writing – review & editing. **Sarael Alcauter:** Writing – review & editing. **Kaspar Schindler:** Data curation, Writing – review & editing. **Roland Wiest:** Data curation, Funding acquisition, Writing – review & editing. **Markus F. Müller:** Conceptualization, Methodology, Validation, Formal analysis, Investigation, Resources, Supervision, Funding acquisition, Writing – original draft, Writing – review & editing. **Christian Rummel:** Conceptualization, Methodology, Validation, Formal analysis, Investigation, Resources, Supervision, Funding acquisition, Writing – original draft, Writing – review & editing.

Acknowledgment

This work was supported by CoNaCyT (grant CF-263377 and CF-610285), the Swiss National Science Foundation (grants 140332 and CRSII5_180365) and the Swiss League Against Epilepsy.

Supplementary material

Supplementary material associated with this article can be found, in the online version, at 10.1016/j.neuroimage.2021.118763

References

Abreu, R., Leal, A., Figueiredo, P., 2018. EEG-informed fMRI: a review of data analysis methods. Front. Hum. Neurosci. 12, 29. doi:10.3389/fnhum.2018.00029.

Allen, P.J., Josephs, O., Turner, R., 2000. A method for removing imaging artifact from continuous EEG recorded during functional MRI. Neuroimage 12 (2), 230–239. doi:10.1006/nimg.2000.0599.

Allen, P.J., Polizzi, G., Krakow, K., Fish, D.R., Lemieux, L., 1998. Identification of EEG events in the mr scanner: the problem of pulse artifact and a method for its subtraction. Neuroimage 8 (3), 229–239.

Andersson, J.L., Jenkinson, M., Smith, S., 2007a. Non-linear optimisation. FMRIB analysis group technical reports. TR07JA1.

Andersson, J. L. R., Jenkinson, M., Smith, S., et al., 2007b. Non-linear registration, AKA spatial normalisation. In: FMRIB Technical Report TR07JA2. Oxford, United Kingdom FMRIB Centre.

Andrzejak, R.G., Schindler, K., Rummel, C., 2012. Nonrandomness, nonlinear dependence, and nonstationarity of electroencephalographic recordings from epilepsy patients. Phys. Rev. E 86 (4), 046206.

Aron, A.R., 2007. The neural basis of inhibition in cognitive control. Neuroscientist 13 (3), 214–228. doi:10.1177/1073858407299288.

Başar, E., Başar-Eroğlu, C., Karakaş, S., Schürmann, M., 1999. Are cognitive processes manifested in event-related gamma, alpha, theta and delta oscillations in the EEG? Neurosci. Lett. 259 (3), 165–168.

Bassett, D.S., Bullmore, E.D., 2006. Small-world brain networks. Neuroscientist 12 (6), 512–523.

Beaty, R.E., Benedek, M., Kaufman, S.B., Silvia, P.J., 2015. Default and executive network coupling supports creative idea production. Sci. Rep. 5 (1), 1–14. doi:10.1038/srep10964.

Beckmann, C.F., Jenkinson, M., Smith, S.M., 2003. General multilevel linear modeling for group analysis in fMRI. Neuroimage 20 (2), 1052–1063.

Beckmann, C.F., Smith, S.M., 2004. Probabilistic independent component analysis for functional magnetic resonance imaging. IEEE Trans. Med. Imaging 23 (2), 137–152.

Beckmann, C.F., Smith, S.M., 2005. Tensorial extensions of independent component analysis for multisubject fMRI analysis. Neuroimage 25 (1), 294–311.

Beggs, J.M., Plenz, D., 2003. Neuronal avalanches in neocortical circuits. J. Neurosci. 23 (35), 11167–11177. doi:10.1523/JNEUROSCI.23-35-11167.2003.

Beggs, J.M., Timme, N., 2012. Being critical of criticality in the brain. Front. Physiol. 3, 163. doi:10.3389/fphys.2012.00163.

Benedek, M., Beaty, R., Jauk, E., Koschutnig, K., Fink, A., Silvia, P.J., Dunst, B., Neubauer, A.C., 2014a. Creating metaphors: the neural basis of figurative language production. Neuroimage 90, 99–106.

Benedek, M., Jauk, E., Fink, A., Koschutnig, K., Reishofer, G., Ebner, F., Neubauer, A.C., 2014b. To create or to recall? Neural mechanisms underlying the generation of creative new ideas. Neuroimage 88, 125–133. doi:10.1016/j.neuroimage.2013.11.021.

Biswal, B., Zerrin Yetkin, F., Haughton, V.M., Hyde, J.S., 1995. Functional connectivity in the motor cortex of resting human brain using echo-planar MRI. Magn. Reson. Med. 34 (4), 537–541.

Blumenfeld, R.S., Parks, C.M., Yonelinas, A.P., Ranganath, C., 2011. Putting the pieces together: the role of dorsolateral prefrontal cortex in relational memory encoding. J. Cogn. Neurosci. 23 (1), 257–265. doi:10.1162/jocn.2010.21459.

Boylan, M.A., Foster, C.M., Pongpipat, E.E., Webb, C.E., Rodrigue, K.M., Kennedy, K.M., 2021. Greater BOLD variability is associated with poorer cognitive function in an adult lifespan sample. Cerebral Cortex 31 (1), 562–574. doi:10.1093/cercor/bhaa243.

Bressler, S.L., Menon, V., 2010. Large-scale brain networks in cognition: emerging methods and principles. Trends Cogn. Sci. 14 (6), 277–290. doi:10.1016/j.tics.2010.04.004.

Bressler, S.L., Tognoli, E., 2006. Operational principles of neurocognitive networks. Int. J. Psychophysiol. 60 (2), 139–148.

Britz, J., Van De Ville, D., Michel, C.M., 2010. Bold correlates of EEG topography reveal rapid resting-state network dynamics. Neuroimage 52 (4), 1162–1170.

Buckner, R.L., Carroll, D.C., 2007. Self-projection and the brain. Trends Cogn. Sci. 11 (2), 49–57. doi:10.1016/j.tics.2006.11.004.

Buckner, R.L., Krienen, F.M., Yeo, B.T.T., 2013. Opportunities and limitations of intrinsic functional connectivity MRI. Nat. Neurosci. 16 (7), 832–837.

Bullmore, E., Sporns, O., 2009. Complex brain networks: graph theoretical analysis of structural and functional systems. Nat. Rev. Neurosci. 10 (3), 186–198.

Buzsaki, G., 2006. Rhythms of the Brain. Oxford University Press.

Centeno, M., Carmichael, D.W., 2014. Network connectivity in epilepsy: resting state fMRI and EEG–fMRI contributions. Front. Neurol. 5, 93. doi:10.3389/fneur.2014.00093.

Chen, J.E., Lewis, L.D., Chang, C., Tian, Q., Fultz, N.E., Ohringer, N.A., Rosen, B.R., Polimeni, J.R., 2020. Resting-state “physiological networks”. Neuroimage 213, 116707. doi:10.1016/j.neuroimage.2020.116707.

Chialvo, D.R., 2007. The brain near the edge. In: AIP Conference Proceedings, Vol. 887. American Institute of Physics, pp. 1–12. doi:10.1063/1.2709580.

Chialvo, D.R., 2010. Emergent complex neural dynamics. Nat. Phys. 6 (10), 744–750.

Chicco, D., Starovoitov, V., Jurman, G., 2021. The benefits of the Matthews correlation coefficient (MCC) over the diagnostic odds ratio (DOR) in binary classification assessment. IEEE Access 9, 47112–47124. doi:10.1109/ACCESS.2021.3068614.

Christoff, K., Gordon, A.M., Smallwood, J., Smith, R., Schooler, J.W., 2009. Experience sampling during fMRI reveals default network and executive system contributions to mind wandering. Proc. Natl. Acad. Sci. 106 (21), 8719–8724. doi:10.1073/pnas.0900234106.

Christov, I.I., 2004. Real time electrocardiogram QRS detection using combined adaptive threshold. Biomed. Eng. Online 3 (1), 28.

Cocchi, L., Gollo, L.L., Zalesky, A., Breakspear, M., 2017. Criticality in the brain: a synthesis of neurobiology, models and cognition. Prog. Neurobiol. 158, 132–152. doi:10.1016/j.pneurobio.2017.07.002.

Cordes, D., Haughton, V.M., Arfanakis, K., Wendt, G.J., Turski, P.A., Moritz, C.H., Quigley, M.A., Meyerand, M.E., 2000. Mapping functionally related regions of brain with functional connectivity MR imaging. Am. J. Neuroradiol. 21 (9), 1636–1644.

Corsi-Cabrera, M., Galindo-Vilchis, L., Del-Río-Portilla, Y., Arce, C., Ramos-Loyo, J., 2007. Within-subject reliability and inter-session stability of EEG power and coherent activity in women evaluated monthly over nine months. Clin. Neurophysiol. 118 (1), 9–21.

Corsi-Cabrera, M., Solis-Ortiz, S., Guevara, M.A., 1997. Stability of EEG inter-and intrahemispheric correlation in women. Electroencephalogr. Clin. Neurophysiol. 102 (3), 248–255.

Curtis, C.E., D’Esposito, M., 2003. Persistent activity in the prefrontal cortex during working memory. Trends Cogn. Sci. 7 (9), 415–423. doi:10.1016/S1364-6613(03)00197-9.

Damoiseaux, J.S., Rombouts, S., Barkhof, F., Scheltens, P., Stam, C.J., Smith, S.M., Beckmann, C.F., 2006. Consistent resting-state networks across healthy subjects. Proc. Natl. Acad. Sci. 103 (37), 13848–13853.

Deichmann, R., Schwarzbauer, C., Turner, R., 2004. Optimisation of the 3d MDEFT sequence for anatomical brain imaging: technical implications at 1.5 and 3 t. Neuroimage 21 (2), 757–767.

Delorme, A., Makeig, S., 2004. Eeglab: an open source toolbox for analysis of single-trial EEG dynamics including independent component analysis. J. Neurosci. Methods 134 (1), 9–21.

Dreher, J.-C., Berman, K.F., 2002. Fractionating the neural substrate of cognitive control processes. Proc. Natl. Acad. Sci. 99 (22), 14595–14600. doi:10.1073/pnas.222193299.

Eguiluz, V.M., Chialvo, D.R., Cecchi, G.A., Baliki, M., Apkarian, A.V., 2005. Scale-free brain functional networks. Phys. Rev. Lett. 94 (1), 018102.

Ellamil, M., Dobson, C., Beeman, M., Christoff, K., 2012. Evaluative and generative modes of thought during the creative process. Neuroimage 59 (2), 1783–1794. doi:10.1016/j.neuroimage.2011.08.008.

Fink, A., Grabner, R.H., Benedek, M., Reishofer, G., Hauswirth, V., Fally, M., Neuper, C., Ebner, F., Neubauer, A.C., 2009. The creative brain: investigation of brain activity during creative problem solving by means of EEG and fMRI. Hum. Brain Mapp. 30 (3), 734–748. doi:10.1002/hbm.20538.

Fink, A., Weber, B., Koschutnig, K., Benedek, M., Reishofer, G., Ebner, F., Papousek, I., Weiss, E.M., 2014. Creativity and Schizotypy from the neuroscience perspective. Cogn. Affect. Behav. Neurosci. 14 (1), 378–387. doi:10.3758/s13415-013-0210-6.

Fox, M.D., Corbetta, M., Snyder, A.Z., Vincent, J.L., Raichle, M.E., 2006. Spontaneous neuronal activity distinguishes human dorsal and ventral attention systems. Proc. Natl. Acad. Sci. 103 (26), 10046–10051.

Fox, M.D., Raichle, M.E., 2007. Spontaneous fluctuations in brain activity observed with functional magnetic resonance imaging. Nat. Rev. Neurosci. 8 (9), 700–711. doi:10.1038/nrn2201.

Fox, M.D., Snyder, A.Z., Vincent, J.L., Corbetta, M., Van Essen, D.C., Raichle, M.E., 2005. The human brain is intrinsically organized into dynamic, anticorrelated functional networks. Proc. Natl. Acad. Sci. 102 (27), 9673–9678. doi:10.1073/pnas.0504136102.

Fox, M.D., Zhang, D., Snyder, A.Z., Raichle, M.E., 2009. The global signal and observed anticorrelated resting state brain networks. J. Neurophysiol. 101 (6), 3270–3283. doi:10.1152/jn.90777.2008.

Fraiman, D., Balenzuela, P., Foss, J., Chialvo, D.R., 2009. Ising-like dynamics in large-scale functional brain networks. Phys. Rev. E 79 (6), 061922. doi:10.1103/PhysRevE.79.061922.

Friston, K.J., Williams, S., Howard, R., Frackowiak, R.S.J., Turner, R., 1996. Movement-related effects in fMRI time-series. Magn. Reson. Med. 35 (3), 346–355. doi:10.1002/mrm.1910350312.

Fuster, J.M., 2000. The module: crisis of a paradigm. Neuron 26 (1), 51–53.

García, A.O.M., Müller, M.F., Schindler, K., Rummel, C., 2013. Genuine cross-correlations: which surrogate based measure reproduces analytical results best? Neural Netw. 46, 154–164.

Garrett, D.D., Kovacevic, N., McIntosh, A.R., Grady, C.L., 2013. The modulation of BOLD variability between cognitive states varies by age and processing speed. Cerebral Cortex 23 (3), 684–693. doi:10.1093/cercor/bhs055.

Ghazanfar, A.A., Schroeder, C.E., 2006. Is neocortex essentially multisensory? Trends Cogn. Sci. 10 (6), 278–285. doi:10.1016/j.tics.2006.04.008.

Glas, A.S., Lijmer, J.G., Prins, M.H., Bonsel, G.J., Bossuyt, P.M.M., 2003. The diagnostic odds ratio: a single indicator of test performance. J. Clin. Epidemiol. 56 (11), 1129–1135.

Goldman, R.I., Stern, J.M., Engel, Cohen, M.S., 2002. Simultaneous EEG and fMRI of the alpha rhythm. Neuroreport 13 (18), 2487.

Gotman, J., 2008. Epileptic networks studied with EEG-fMRI. Epilepsia 49, 42–51.

Gotman, J., Kobayashi, E., Bagshaw, A.P., Bénar, C.-G., Dubeau, F., 2006. Combining EEG and fMRI: a multimodal tool for epilepsy research. J. Magn. Reson. Imaging Off. J. Int. Soc. Magn. Reson. Med. 23 (6), 906–920. doi:10.1002/jmri.20577.

Goulden, N., Khusnulina, A., Davis, N.J., Bracewell, R.M., Bokde, A.L., McNulty, J.P., Mullins, P.G., 2014. The salience network is responsible for switching between the default mode network and the central executive network: replication from DCM. Neuroimage 99, 180–190. doi:10.1016/j.neuroimage.2014.05.052.

van Graan, L.A., Lemieux, L., Chaudhary, U.J., 2015. Methods and utility of EEG-fMRI in epilepsy. Quant. Imaging Med. Surg. 5 (2), 300. doi:10.3978/j.issn.2223-4292.2015.02.04.

Grady, C.L., Garrett, D.D., 2014. Understanding variability in the BOLD signal and why it matters for aging. Brain Imaging Behav. 8 (2), 274–283. doi:10.1007/s11682-013-9253-0.

Greicius, M.D., Krasnow, B., Reiss, A.L., Menon, V., 2003. Functional connectivity in the resting brain: a network analysis of the default mode hypothesis. Proc. Natl. Acad. Sci. 100 (1), 253–258.

Greve, D.N., Fischl, B., 2009. Accurate and robust brain image alignment using boundary-based registration. Neuroimage 48 (1), 63–72.

Hastings, H.M., 1984. Stability of large systems. BioSystems 17 (2), 171–177.

He, B.J., Snyder, A.Z., Zempel, J.M., Smyth, M.D., Raichle, M.E., 2008. Electrophysiological correlates of the brain’s intrinsic large-scale functional architecture. Proc. Natl. Acad. Sci. 105 (41), 16039–16044.

Held, P., Fellner, C., Fellner, F., Geissler, A., Gmeinwieser, J., 1995. Three-dimensional MP-RAGE-an alternative to conventional three-dimensional FLASH sequences for the diagnosis of viscerocranial tumours? Br. J. Radiol. 68 (816), 1316–1324.
Hellyer, P.J., Shanahan, M., Scott, G., Wise, R.J.S., Sharp, D.J., Leech, R., 2014. The control of global brain dynamics: opposing actions of frontoparietal control and default mode networks on attention. J. Neurosci. 34 (2), 451–461. doi:10.1523/JNEUROSCI.1853-13.2014.
Horovitz, S.G., Fukunaga, M., de Zwart, J.A., van Gelderen, P., Fulton, S.C., Balkin, T.J., Duyn, J.H., 2008. Low frequency bold fluctuations during resting wakefulness and light sleep: a simultaneous EEG-fMRI study. Hum. Brain Mapp. 29 (6), 671–682.
Hyvarinen, A., 1999. Fast and robust fixed-point algorithms for independent component analysis. IEEE Trans. Neural Netw. 10 (3), 626–634.
Iannetti, G.D., Niazy, R.K., Wise, R.G., Jezzard, P., Brooks, J.C.W., Zambreanu, L., Vennart, W., Matthews, P.M., Tracey, I., 2005. Simultaneous recording of laser-evoked brain potentials and continuous, high-field functional magnetic resonance imaging in humans. Neuroimage 28 (3), 708–719.
Jann, K., Dierks, T., Boesch, C., Kottlow, M., Strik, W., Koenig, T., 2009. Bold correlates of EEG alpha phase-locking and the fMRI default mode network. Neuroimage 45 (3), 903–916.
Jann, K., Kottlow, M., Dierks, T., Boesch, C., Koenig, T., 2010. Topographic electrophysiological signatures of fMRI resting state networks. PLoS ONE 5 (9), e12945.
Jann, K., Wiest, R., Hauf, M., Meyer, K., Boesch, C., Mathis, J., Schroth, G., Dierks, T., Koenig, T., 2008. Bold correlates of continuously fluctuating epileptic activity isolated by independent component analysis. Neuroimage 42 (2), 635–648.
Jenkinson, M., Bannister, P., Brady, M., Smith, S., 2002. Improved optimization for the robust and accurate linear registration and motion correction of brain images. Neuroimage 17 (2), 825–841.
Jenkinson, M., Smith, S., 2001. A global optimisation method for robust affine registration of brain images. Med. Image Anal. 5 (2), 143–156.
Kaiser, J., Lutzenberger, W., 2005. Human gamma-band activity: a window to cognitive processing. Neuroreport 16 (3), 207–211.
Kello, C.T., Brown, G.D.A., Ferrer-i Cancho, R., Holden, J.G., Linkenkaer-Hansen, K., Rhodes, T., Van Orden, G.C., 2010. Scaling laws in cognitive sciences. Trends Cogn. Sci. 14 (5), 223–232. doi:10.1016/j.tics.2010.02.005.
Kramer, M.A., Eden, U.T., Lepage, K.Q., Kolaczyk, E.D., Bianchi, M.T., Cash, S.S., 2011. Emergence of persistent networks in long-term intracranial EEG recordings. J. Neurosci. 31 (44), 15757–15767.
Labounek, R., Bridwell, D.A., Mareček, R., Lamoš, M., Mikl, M., Bednařík, P., Baštinec, J., Slavíček, T., Hluštík, P., Brázdil, M., et al., 2019. Eeg spatiospectral patterns and their link to fMRI bold signal via variable hemodynamic response functions. J. Neurosci. Methods 318, 34–46.
Laloux, L., Cizeau, P., Bouchaud, J.-P., Potters, M., 1999. Noise dressing of financial correlation matrices. Phys. Rev. Lett. 83 (7), 1467.
Lancaster, G., Iatsenko, D., Pidde, A., Ticcinelli, V., Stefanovska, A., 2018. Surrogate data for hypothesis testing of physical systems. Phys. Rep. 748, 1–60.
Laufs, H., Kleinschmidt, A., Beyerle, A., Eger, E., Salek-Haddadi, A., Preibisch, C., Krakow, K., 2003. EEG-correlated fMRI of human alpha activity. Neuroimage 19 (4), 1463–1476.
Lemieux, L., Allen, P.J., Franconi, F., Symms, M.R., Fish, D.K., 1997. Recording of EEG during fMRI experiments: patient safety. Magn. Reson. Med. 38 (6), 943–952.
Linkenkaer-Hansen, K., Nikouline, V.V., Palva, J.M., Ilmoniemi, R.J., 2001. Long-range temporal correlations and scaling behavior in human brain oscillations. J. Neurosci. 21 (4), 1370–1377.
Manoliu, A., Riedl, V., Zherdin, A., Mühlau, M., Schwerthöffer, D., Scherr, M., Peters, H., Zimmer, C., Förstl, H., Bäuml, J., et al., 2014. Aberrant dependence of default mode/central executive network interactions on anterior insular salience network activity in schizophrenia. Schizophr. Bull. 40 (2), 428–437. doi:10.1093/schbul/sbt037.
Mantini, D., Perrucci, M.G., Del Gratta, C., Romani, G.L., Corbetta, M., 2007. Electrophysiological signatures of resting state networks in the human brain. Proc. Natl. Acad. Sci. 104 (32), 13170–13175.
de Manzano, O., Ullén, F., 2012. Goal-independent mechanisms for free response generation: creative and pseudo-random performance share neural substrates. Neuroimage 59 (1), 772–780.
Marstaller, L., Fynes-Clinton, S., Burianová, H., Reutens, D.C., 2021. Salience and default-mode network connectivity during threat and safety processing in older adults. Hum. Brain Mapp. 42 (1), 14–23. doi:10.1002/hbm.25199.
Mason, M.F., Norton, M.I., Van Horn, J.D., Wegner, D.M., Grafton, S.T., Macrae, C.N., 2007. Wandering minds: the default network and stimulus-independent thought. Science 315 (5810), 393–395. doi:10.1126/science.1131295.
Mayeli, A., Al Zoubi, O., Henry, K., Wong, C.K., White, E., Luo, Q., Zotev, V., Refai, H., Bodurka, J.A., 2021. Automated pipeline for EEG artifact reduction (APPEAR) recorded during fMRI. J. Neural Eng. 18, 0460b4. doi:10.1088/1741-2552/ac1037.
McIntosh, A.R., Kovacevic, N., Lippe, S., Garrett, D., Grady, C., Jirsa, V., 2010. The development of a noisy brain. Arch. Ital. Biol. 148 (3), 323–337. doi:10.4449/aib.v148i3.1225.
McMillan, R., Kaufman, S.B., Singer, J.L., 2013. Ode to positive constructive daydreaming. Front. Psychol. 4, 626. doi:10.3389/fpsyg.2013.00626.
Menon, V., 2011. Large-scale brain networks and psychopathology: a unifying triple network model. Trends Cogn. Sci. 15 (10), 483–506. doi:10.1016/j.tics.2011.08.003.
Menon, V., Uddin, L.Q., 2010. Saliency, switching, attention and control: a network model of insula function. Brain Struct. Funct. 214 (5–6), 655–667. doi:10.1007/s00429-010-0262-0.
Michel, C.M., Koenig, T., 2018. Eeg microstates as a tool for studying the temporal dynamics of whole-brain neuronal networks: a review. Neuroimage 180, 577–593.
Millar, P.R., Petersen, S.E., Ances, B.M., Gordon, B.A., Benzinger, T.L.S., Morris, J.C., Balota, D.A., 2020. Evaluating the sensitivity of resting-state BOLD variability to age and cognition after controlling for motion and cardiovascular influences: a network-based approach. Cerebral Cortex 30 (11), 5686–5701. doi:10.1093/cercor/bhaa138.
Mišic, B., Mills, T., Taylor, M.J., McIntosh, A.R., 2010. Brain noise is task dependent and region specific. J. Neurophysiol. 104 (5), 2667–2676. doi:10.1152/jn.00648.2010.
Müller, M.F., Baier, G., Jiménez, Y.L., García, A.O.M., Rummel, C., Schindler, K., 2011. Evolution of genuine cross-correlation strength of focal onset seizures. J. Clin. Neurophysiol. 28 (5), 450–462.
Müller, M.F., Rummel, C., Goodfellow, M., Schindler, K., 2014. Standing waves as an explanation for generic stationary correlation patterns in noninvasive EEG of focal onset seizures. Brain Connect. 4 (2), 131–144. doi:10.1089/brain.2013.0192.
Münnix, M.C., Shimada, T., Schäfer, R., Leyvraz, F., Seligman, T.H., Guhr, T., Stanley, H.E., 2012. Identifying states of a financial market. Sci. Rep. 2, 644.
Neuner, I., Arrubla, J., Werner, C.J., Hitz, K., Boers, F., Kawohl, W., Shah, N.J., 2014. The default mode network and EEG regional spectral power: a simultaneous fMRI-EEG study. PLoS One 9 (2), e88214.
Niazy, R.K., Beckmann, C.F., Iannetti, G.D., Brady, J.M., Smith, S.M., 2005. Removal of fMRI environment artifacts from EEG data using optimal basis sets. Neuroimage 28 (3), 720–737.
Niazy, R.K., Iannetti, G., Beckmann, C.F., Brady, M., Smith, S.M., 1999. Improved fMRI artifact reduction from simultaneously acquired EEG data using slice dependant template matching. Neuroreport 80 (4).
Nunez, P.L., Silberstein, R.B., 2000. On the relationship of synaptic activity to macroscopic measurements: does co-registration of EEG with fMRI make sense? Brain Topogr. 13 (2), 79–96. doi:10.1023/A:1026683200895.
Olguín-Rodríguez, P.V., Arzate-Mena, J.D., Corsi-Cabrera, M., Gast, H., Marín-García, A., Mathis, J., Ramos Loyo, J., del Rio-Portilla, I.Y., Rummel, C., Schindler, K., et al., 2018. Characteristic fluctuations around stable attractor dynamics extracted from highly nonstationary electroencephalographic recordings. Brain Connect. 8 (8), 457–474. doi:10.1089/brain.2018.0609.
Palva, J.M., Zhigalov, A., Hirvonen, J., Korhonen, O., Linkenkaer-Hansen, K., Palva, S., 2013. Neuronal long-range temporal correlations and avalanche dynamics are correlated with behavioral scaling laws. Proc. Natl. Acad. Sci. 110 (9), 3585–3590. doi:10.1073/pnas.1216855110.
Petermann, T., Thiagarajan, T.C., Lebedev, M.A., Nicolelis, M.A.L., Chialvo, D.R., Plenz, D., 2009. Spontaneous cortical activity in awake monkeys composed of neuronal avalanches. Proc. Natl. Acad. Sci. 106 (37), 15921–15926. doi:10.1073/pnas.0904089106.
Pievani, M., de Haan, W., Wu, T., Seeley, W.W., Frisoni, G.B., 2011. Functional network disruption in the degenerative dementias. Lancet Neurol. 10 (9), 829–843. doi:10.1016/S1474-4422(11)70158-2.
Pittau, F., Grova, C., Moeller, F., Dubeau, F., Gotman, J., 2012. Patterns of altered functional connectivity in mesial temporal lobe epilepsy. Epilepsia 53 (6), 1013–1023. doi:10.1111/j.1528-1167.2012.03464.x.
Plerou, V., Gopikrishnan, P., Rosenow, B., Amaral, L.A.N., Stanley, H.E., 1999. Universal and nonuniversal properties of cross correlations in financial time series. Phys. Rev. Lett. 83 (7), 1471.
Poil, S.-S., Hardstone, R., Mansvelder, H.D., Linkenkaer-Hansen, K., 2012. Critical-state dynamics of avalanches and oscillations jointly emerge from balanced excitation/inhibition in neuronal networks. J. Neurosci. 32 (29), 9817–9823. doi:10.1523/JNEUROSCI.5990-11.2012.
Poil, S.-S., van Ooyen, A., Linkenkaer-Hansen, K., 2008. Avalanche dynamics of human brain oscillations: relation to critical branching processes and temporal correlations. Hum. Brain Mapp. 29 (7), 770–777. doi:10.1002/hbm.20590.
Portnova, G.V., Tetereva, A., Balaev, V., Atanov, M., Skiteva, L., Ushakov, V., Ivanitsky, A., Martynova, O., 2018. Correlation of BOLD signal with linear and nonlinear patterns of EEG in resting state EEG-informed fMRI. Front. Hum. Neurosci. 11, 654.
Prestel, M., Steinfath, T.P., Tremmel, M., Stark, R., Ott, U., 2018. FMRI BOLD correlates of EEG independent components: spatial correspondence with the default mode network. Front. Hum. Neurosci. 12, 478. doi:10.3389/fnhum.2018.00478.
Preti, M.G., Bolton, T.A.W., Van De Ville, D., 2017. The dynamic functional connectome: state-of-the-art and perspectives. Neuroimage 160, 41–54.
Raichle, M.E., 2006. The Brain's dark energy. Sci. N.Y. Washington- 314 (5803), 1249. doi:10.1126/science. 1134405.
Raichle, M.E., 2011. The restless brain. Brain Connect. 1 (1), 3–12. doi:10.1089/brain.2011.0019.
Raichle, M.E., MacLeod, A.M., Snyder, A.Z., Powers, W.J., Gusnard, D.A., Shulman, G.L., 2001. A default mode of brain function. Proc. Natl. Acad. Sci. 98 (2), 676–682.
Raichle, M.E., Mintun, M.A., 2006. Brain work and brain imaging. Annu. Rev. Neurosci. 29, 449–476.
Rajkumar, R., Farrher, E., Mauler, J., Sripad, P., Régio Brambilla, C., Rota Kops, E., Scheins, J., Dammers, J., Lerche, C., Langen, K.-J., et al., 2018. Comparison of EEG microstates with resting state fMRI and FDG-PET measures in the default mode network via simultaneously recorded trimodal (PET/MR/EEG) data. Hum. Brain Mapp. doi:10.1002/hbm.24429.
Rios, W.A., Olguín, P.V., Mena, D.A., Cabrera, M.C., Escalona, J., Garcia, A.M., Loyo, J.R., LOPEZ, D.R., Zapata, J.F., Müller, M., et al., 2019. The influence of EEG references on the analysis of spatio-temporal interrelation patterns. Front. Neurosci. 13, 941. doi:10.3389/fnins.2019.00941.
Ritter, P., Villringer, A., 2006. Simultaneous EEG–fMRI. Neurosci. Biobehav. Rev. 30 (6), 823–838. doi:10.1016/j.neubiorev.2006.06.008.
Rummel, C., Müller, M., Baier, G., Amor, F., Schindler, K., 2010. Analyzing spatio-temporal patterns of genuine cross-correlations. J. Neurosci. Methods 191 (1), 94–100.
Samogin, J., Liu, Q., Marino, M., Wenderoth, N., Mantini, D., 2019. Shared and connection-specific intrinsic interactions in the default mode network. Neuroimage 200, 474–481. doi:10.1016/j.neuroimage.2019.07.007.
Schacter, D.L., Addis, D.R., Hassabis, D., Martin, V.C., Spreng, R.N., Szpunar, K.K., 2012.

The future of memory: remembering, imagining, and the brain. Neuron 76 (4), 677–694. doi:10.1016/j.neuron.2012.11.001.
Schelter, B., Timmer, J., Schulze-Bonhage, A., 2008. Seizure Prediction in Epilepsy. Wiley Online Library.
Schneider, M., Somers, M., 2006. Organizations as complex adaptive systems: implications of complexity theory for leadership research. Leadersh. Q. 17 (4), 351–365.
Schreiber, T., Schmitz, A., 1996. Improved surrogate data for nonlinearity tests. Phys. Rev. Lett. 77 (4), 635–638. doi:10.1103/PhysRevLett.77.635. 9909041
Schreiber, T., Schmitz, A., 2000. Surrogate time series. Phys. D 142 (3–4), 346–382. doi:10.1016/S0167-2789(00)00043-9. 9909037
Seeley, W.W., Menon, V., Schatzberg, A.F., Keller, J., Glover, G.H., Kenna, H., Reiss, A.L., Greicius, M.D., 2007. Dissociable intrinsic connectivity networks for salience processing and executive control. J. Neurosci. 27 (9), 2349–2356. doi:10.1523/JNEUROSCI.5587-06.2007.
Seitzman, B.A., Snyder, A.Z., Leuthardt, E.C., Shimony, J.S., 2019. The state of resting state networks. Top. Magn. Reson. Imaging 28 (4), 189–196.
Singer, W., 1993. Synchronization of cortical activity and its putative role in information processing and learning. Annu. Rev. Physiol. 55 (1), 349–374.
Singer, W., 2013. Cortical dynamics revisited. Trends Cogn. Sci. 17 (12), 616–626.
Smith, S.M., 2002. Fast robust automated brain extraction. Hum. Brain Mapp. 17 (3), 143–155.
Smith, S.M., Fox, P.T., Miller, K.L., Glahn, D.C., Fox, P.M., Mackay, C.E., Filippini, N., Watkins, K.E., Toro, R., Laird, A.R., et al., 2009. Correspondence of the brain's functional architecture during activation and rest. Proc. Natl. Acad. Sci. 106 (31), 13040–13045.
Sporns, O., Kötter, R., 2004. Motifs in brain networks. PLoS Biol. 2 (11), e369. doi:10.1371/journal.pbio.0020369.
Sporns, O., Tononi, G., Edelman, G.M., 2000. Theoretical neuroanatomy: relating anatomical and functional connectivity in graphs and cortical connection matrices. Cerebral Cortex 10 (2), 127–141.
Sridharan, D., Levitin, D.J., Menon, V., 2008. A critical role for the right fronto-insular cortex in switching between central-executive and default-mode networks. Proc. Natl. Acad. Sci. 105 (34), 12569–12574. doi:10.1073/pnas.0800005105.
Tagliazucchi, E., Balenzuela, P., Fraiman, D., Chialvo, D.R., 2012. Criticality in large-scale brain fMRI dynamics unveiled by a novel point process analysis. Front. Physiol. 3, 15.
Tagliazucchi, E., Chialvo, D. R., The collective brain is critical. arXiv preprint arXiv:1103.2070
Takeuchi, H., Taki, Y., Hashizume, H., Sassa, Y., Nagase, T., Nouchi, R., Kawashima, R., 2011. Failing to deactivate: the association between brain activity during a working memory task and creativity. Neuroimage 55 (2), 681–687. doi:10.1016/j.neuroimage.2010.11.052.
Tzourio-Mazoyer, N., Landeau, B., Papathanassiou, D., Crivello, F., Etard, O., Delcroix, N., Mazoyer, B., Joliot, M., 2002. Automated anatomical labeling of activations in SPM using a macroscopic anatomical parcellation of the MNI MRI single-subject brain. Neuroimage 15 (1), 273–289.
Van Den Heuvel, M.P., Pol, H.E.H., 2010. Exploring the brain network: a review on resting-state fMRI functional connectivity. Eur. Neuropsychopharmacol. 20 (8), 519–534.
Vidaurre, D., Smith, S.M., Woolrich, M.W., 2017. Brain network dynamics are hierarchically organized in time. Proc. Natl. Acad. Sci. 114 (48), 12827–12832. doi:10.1073/pnas.1705120114.
Whitham, E.M., Pope, K.J., Fitzgibbon, S.P., Lewis, T., Clark, C.R., Loveless, S., Broberg, M., Wallace, A., DeLosAngeles, D., Lillie, P., et al., 2007. Scalp electrical recording during paralysis: quantitative evidence that EEG frequencies above 20 hz are contaminated by EMG. Clin. Neurophysiol. 118 (8), 1877–1888. doi:10.1016/j.clinph.2007.04.027.
Wiest, R., Abela, E., Rummel, C., 2015. Simultaneous EEG-fMRI in epilepsy. In: Clinical Functional MRI. Springer, pp. 159–177.
Wiest, R., Estermann, L., Scheidegger, O., Rummel, C., Jann, K., Seeck, M., Schindler, K., Hauf, M., 2013. Widespread grey matter changes and hemodynamic correlates to interictal epileptiform discharges in pharmacoresistant mesial temporal epilepsy. J. Neurol. 260 (6), 1601–1610.
Wollin, D., Perry, C., 2004. Marketing management in a complex adaptive system. Eur. J. Mark. 38 (5/6), 556–572. doi:10.1108/03090560410529213.
Woolrich, M., 2008. Robust group analysis using outlier inference. Neuroimage 41 (2), 286–301.
Woolrich, M.W., Behrens, T.E.J., Beckmann, C.F., Jenkinson, M., Smith, S.M., 2004. Multilevel linear modelling for fMRI group analysis using Bayesian inference. Neuroimage 21 (4), 1732–1747.
Woolrich, M.W., Ripley, B.D., Brady, M., Smith, S.M., 2001. Temporal autocorrelation in univariate linear modeling of FMRI data. Neuroimage 14 (6), 1370–1386.
Worsley, K.J., 2001. 14 Statistical analysis of activation images. Funct. MRI Int. Methods 251.
Yang, H., Shew, W.L., Roy, R., Plenz, D., 2012. Maximal variability of phase synchrony in cortical networks with neuronal avalanches. J. Neurosci. 32 (3), 1061–1072. doi:10.1523/JNEUROSCI.2771-11.2012.
Yuan, H., Zotev, V., Phillips, R., Bodurka, J., 2013. Correlated slow fluctuations in respiration, EEG, and BOLD fMRI. Neuroimage 79, 81–93. doi:10.1016/j.neuroimage.2013.04.068.
Zang, Y.-F., Zhao, S.-G., et al., 2012. Resting-state fMRI studies in epilepsy. Neurosci. Bull. 28 (4), 449–455.
Zhang, L., Zuo, X.-N., Ng, K.K., Chong, J.S.X., Shim, H.Y., Ong, M.Q.W., Loke, Y.M., Choo, B.L., Chong, E.J.Y., Wong, Z.X., et al., 2020. Distinct BOLD variability changes in the default mode and salience networks in Alzheimer's disease spectrum and associations with cognitive decline. Sci. Rep. 10 (1), 1–12. doi:10.1038/s41598-020-63540-4.